Haloes gone MAD[*]: The Halo-Finder Comparison Project

Alexander Knebe,[1][†] Steffen R. Knollmann,[1] Stuart I. Muldrew,[2] Frazer R. Pearce,[2]
Miguel Angel Aragon-Calvo,[3] Yago Ascasibar,[1] Peter S. Behroozi,[4,5,6]
Daniel Ceverino,[7] Stephane Colombi,[8] Juerg Diemand,[9] Klaus Dolag,[10]
Bridget L. Falck,[3] Patricia Fasel,[11] Jeff Gardner,[12] Stefan Gottlöber,[13]
Chung-Hsing Hsu,[14] Francesca Iannuzzi,[10] Anatoly Klypin,[15] Zarija Lukić,[16]
Michal Maciejewski,[10] Cameron McBride,[17] Mark C. Neyrinck,[3] Susana Planelles,[18]
Doug Potter,[9] Vicent Quilis,[18] Yann Rasera,[19] Justin I. Read,[20,21] Paul M. Ricker,[22,23]
Fabrice Roy,[19] Volker Springel,[24,25] Joachim Stadel,[9] Greg Stinson,[26] P. M. Sutter,[22]
Victor Turchaninov,[27] Dylan Tweed,[28] Gustavo Yepes[1] and Marcel Zemp[29]

[1]*Departamento de Física Teórica, Módulo C-15, Facultad de Ciencias, Universidad Autónoma de Madrid, 28049 Cantoblanco, Madrid, Spain*
[2]*School of Physics & Astronomy, University of Nottingham, Nottingham NG7 2RD*
[3]*Department of Physics and Astronomy, Johns Hopkins University, 3701 San Martin Drive, Baltimore, MD 21218, USA*
[4]*Kavli Institute for Particle Astrophysics and Cosmology, Stanford, CA 94309, USA*
[5]*Physics Department, Stanford University, Stanford, CA 94305, USA*
[6]*SLAC National Accelerator Laboratory, Menlo Park, CA 94025, USA*
[7]*Racah Institute of Physics, The Hebrew University, Jerusalem 91904, Israel*
[8]*Institut d'Astrophysique de Paris, CNRS UMR 7095 and UPMC, 98bis, bd Arago, F-75014 Paris, France*
[9]*Institute for Theoretical Physics, University of Zurich, Winterthurerstrasse 190, CH-8057 Zurich, Switzerland*
[10]*Max-Planck Institut für Astrophysik, Karl-Schwarzschild Str. 1, D-85741 Garching, Germany*
[11]*CCS-3, Computer, Computational and Statistical Sciences Division, Los Alamos National Laboratory, PO Box 1663, Los Alamos, NM 87544, USA*
[12]*Department of Physics, University of Washington, PO Box 351560, Seattle, WA 98195, USA*
[13]*Astrophysikalisches Institut Potsdam, An der Sternwarte 16, 14482 Potsdam, Germany*
[14]*Computer Science and Mathematics Division, Oak Ridge National Laboratory, PO Box 2008, Oak Ridge, TN 37831, USA*
[15]*Department of Astronomy, New Mexico State University, Las Cruces, NM 88003-0001, USA*
[16]*T-2, Theoretical Division, Los Alamos National Laboratory, PO Box 1663, Los Alamos, NM 87544, USA*
[17]*Department of Physics & Astronomy, Vanderbilt University, 6301 Stevenson Center, Nashville, TN 37235, USA*
[18]*Departament d'Astronomia i Astrofísica, Universitat de València, 46100 - Burjassot (Valencia), Spain*
[19]*CNRS, Laboratoire Univers et Théories (LUTh), UMR 8102 CNRS, Observatoire de Paris, Université Paris Diderot, 5 Place Jules Janssen, 92190 Meudon, France*
[20]*Institute for Astronomy, Department of Physics, ETH Zürich, Wolfgang-Pauli-Strasse 16, CH-8093 Zürich, Switzerland*
[21]*Department of Physics and Astronomy, University of Leicester, University Road, Leicester LE1 7RH*
[22]*Department of Physics, University of Illinois at Urbana-Champaign, Urbana, IL 61801-3080, USA*
[23]*National Center for Supercomputing Applications, University of Illinois at Urbana-Champaign, Urbana, IL 61801, USA*
[24]*Heidelberg Institute for Theoretical Studies, Schloss-Wolfsbrunnenweg 35, 69118 Heidelberg, Germany*
[25]*Zentrum für Astronomie der Universität Heidelberg, ARI, Mönchhofstr. 12-14, 69120 Heidelberg, Germany*
[26]*Jeremiah Horrocks Institute, University of Central Lancashire, Preston PR1 2HE*
[27]*Keldysh Institute of Applied Mathematics, Russian Academy of Sciences, 125047 Moscow, Russia*
[28]*Institut d'Astrophysique Spatiale, CNRS/Universite Paris-Sud 11, 91405 Orsay, France*
[29]*Department of Astronomy, University of Michigan, 500 Church Street, Ann Arbor, MI 48109-1042, USA*

ABSTRACT

We present a detailed comparison of fundamental dark matter halo properties retrieved by a substantial number of different halo finders. These codes span a wide range of techniques including friends-of-friends, spherical-overdensity and phase-space-based algorithms. We

[*] Airport code for Madrid, Spain
[†] E-mail: alexander.knebe@uam.es

further introduce a robust (and publicly available) suite of test scenarios that allow halo finder developers to compare the performance of their codes against those presented here. This set includes mock haloes containing various levels and distributions of substructure at a range of resolutions as well as a cosmological simulation of the large-scale structure of the universe.

All the halo-finding codes tested could successfully recover the spatial location of our mock haloes. They further returned lists of particles (potentially) belonging to the object that led to coinciding values for the maximum of the circular velocity profile and the radius where it is reached. All the finders based in configuration space struggled to recover substructure that was located close to the centre of the host halo, and the radial dependence of the mass recovered varies from finder to finder. Those finders based in phase space could resolve central substructure although they found difficulties in accurately recovering its properties. Through a resolution study we found that most of the finders could not reliably recover substructure containing fewer than 30–40 particles. However, also here the phase-space finders excelled by resolving substructure down to 10–20 particles. By comparing the halo finders using a high-resolution cosmological volume, we found that they agree remarkably well on fundamental properties of astrophysical significance (e.g. mass, position, velocity and peak of the rotation curve).

We further suggest to utilize the peak of the rotation curve, v_{max}, as a proxy for mass, given the arbitrariness in defining a proper halo edge.

Key words: methods: numerical – galaxies: evolution – galaxies: haloes – cosmology: miscellaneous – cosmology: theory – dark matter.

1 INTRODUCTION

While recent decades have seen great progress in the understanding and modelling of the large- and small-scale structure of the Universe by means of numerical simulations, there remains one very fundamental question that is yet to be answered: 'how to find a dark matter (DM) halo?' The comparison of any cosmological simulation to observational data relies upon reproducibly identifying 'objects' within the model. But how do we identify 'DM haloes' or even 'galaxies' in such simulations? Researchers in the field have developed a wide variety of techniques and codes to accomplish this task. But how does the performance of these various techniques and codes compare? While we still may argue about the proper definition of an 'object', the various approaches should nevertheless agree, once the same recipe for defining a (DM) halo is used.

This introduction begins by establishing why it is important to have 'The Halo-Finder Comparison Project' before continuing by laying out the groundwork for the comparison we have undertaken. It is therefore subdivided into a first subsection where we highlight the necessity for such a comparison and summarize the recent literature in this area. This section also includes a brief primer on halo finders and their history. The second part introduces the design of the test cases, illustrated with some analysis. The last part then raises the question 'how to cross-compare haloes?' as well as 'what is actually a halo?' and presents a possible answer the authors agreed upon.

1.1 The necessity for a comparison project

Over the last 30 years, great progress has been made in the development of simulation codes that model the distribution of dissipationless DM while simultaneously following the (substantially more complex) physics of the baryonic component that accounts for the observable Universe. Nowadays, we have a great variety of highly reliable, cost-effective (and sometimes publicly available) codes designed for the simulation of cosmic structure formation

(e.g. Couchman, Thomas & Pearce 1995; Gnedin 1995; Pen 1995; Kravtsov, Klypin & Khokhlov 1997; Bode, Ostriker & Xu 2000; Fryxell et al. 2000; Knebe, Green & Binney 2001; Springel, Yoshida & White 2001b; Teyssier 2002; Dubinski et al. 2004; O'Shea et al. 2004; Quilis 2004; Merz, Pen & Trac 2005; Springel 2005; Bagla & Khandai 2009; Doumler & Knebe 2010; Springel 2010).

However, producing the (raw) simulation data is only the first step in the process; the model requires reduction before it can be compared to the observed Universe we inhabit. This necessitates access to analysis tools to map the data onto 'real' objects; traditionally, this has been accomplished via the use of 'halo finders'. Conventional halo finders search the (dark) matter density field within the simulations generated by the aforementioned codes to find locally overdense gravitationally bound systems, which are then tagged as (dark) matter haloes. Such tools have led to critical insights into our understanding of the origin and evolution of cosmic structure. To take advantage of sophisticated simulation codes and to optimize their predictive power, one obviously needs equally sophisticated halo finders! Therefore, this field has also seen great development in recent years (e.g. Gelb & Bertschinger 1994; Klypin & Holtzman 1997; Eisenstein & Hut 1998; Bullock et al. 2001; Springel et al. 2001a; Stadel 2001; Aubert et al. 2004; Gill et al. 2004; Neyrinck et al. 2005; Weller et al. 2005; Diemand et al. 2006; Kim & Park 2006; Gardner et al. 2007a,b; Shaw et al. 2007; Habib et al. 2009; Knollmann & Knebe 2009; Maciejewski et al. 2009; Ascasibar, in preparation; Behroozi, in preparation; Planelles & Quilis 2010; Rasera et al. 2010; Skory et al. 2010; Sutter & Ricker 2010; Falck et al., in preparation; see also Fig. 1, noting that for some halo finders no code paper exists yet). However, so far, comparison projects have tended to focus on the simulation codes themselves rather than the analysis tools.

The increasing demand and supply for halo finders is schematically presented in Fig. 1 where we show the (cumulative) number of codes as a function of time, binned in 10-yr intervals since 1970. We can clearly see the increasing pace of development in the past decade, reflecting the necessity for sophisticated codes: in the last
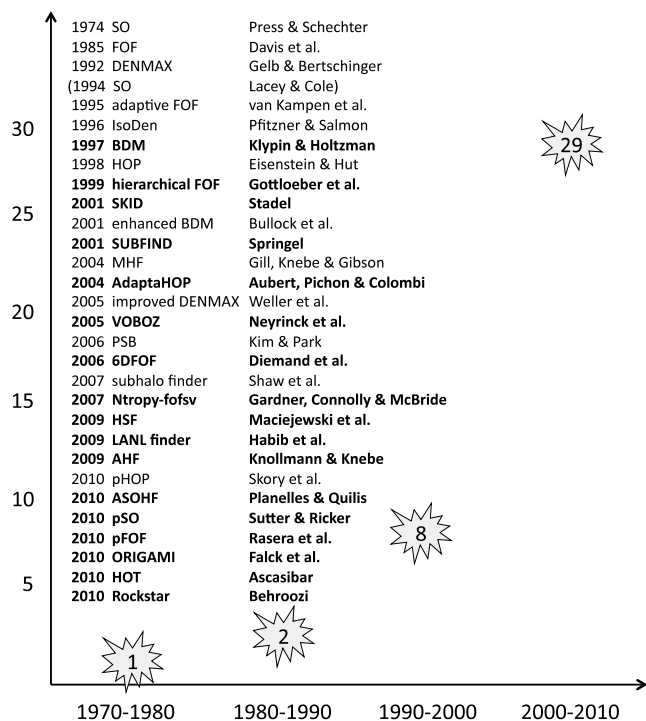
Figure 1. Schematic presentation of the (cumulative) number of halo finders as a function of time, binned in 10-yr intervals since 1970. The codes participating in this comparison project have been highlighted in bold font.

10 years, the number of existing halo-finding codes has practically tripled. While for a long time the spherical-overdensity (SO) method first mentioned by Press & Schechter (1974) as well as the friend-of-friends (FOF) algorithm introduced by Davis et al. (1985) remained the standard techniques, the situation changed in the 1990s when new methods were developed (Gelb 1992; Lacey & Cole 1994; van Kampen 1995; Pfitzner & Salmon 1996; Klypin & Holtzman 1997; Eisenstein & Hut 1998; Gottlöber, Klypin & Kravtsov 1999).

While the first generation of halo finders primarily focused on identifying isolated field haloes, the situation dramatically changed, once it became clear that there was no such thing as 'overmerging', that is, the premature destruction of haloes orbiting inside larger host haloes (Klypin et al. 1999) was a numerical artefact rather than a real physical process. Now codes faced the challenge of finding both haloes embedded within the (more or less uniform) background density of the Universe and subhaloes orbiting within a density gradient of a larger host halo. The past decade has seen a substantial number of codes and techniques introduced in an attempt to cope with this problem (Bullock et al. 2001; Springel et al. 2001a; Stadel 2001; Aubert et al. 2004; Gill et al. 2004; Neyrinck et al. 2005; Weller et al. 2005; Diemand et al. 2006; Kim & Park 2006; Gardner et al. 2007a,b; Shaw et al. 2007; Knollmann & Knebe 2009; Maciejewski et al. 2009; Planelles & Quilis 2010). Along with the need to identify subhaloes, simulations became much larger during this period and this led to a drive towards parallel analysis tools. The simulation data had become too large to be analysed on single CPU architectures and hence halo finders had to be developed to cope with this situation, too.

Nevertheless, the first two halo finders mentioned in the literature, that is, the SO method (Press & Schechter 1974) and the FOF algorithm (Davis et al. 1985) remain the foundation of nearly every code: they often involve at least one phase where either particles are linked together or (spherical) shells are grown to collect particles.

While we do not wish to invent stereotypes or a classification scheme for halo finders, there are unarguably two distinct groups of codes:

(i) density peak locator (+ particle collection); and
(ii) particle collector.

The density peak locators – such as the classical SO method – aim at identifying by whatever means peaks in the matter density field. About these centres, (spherical) shells are grown out to the point where the density profile drops below a certain pre-defined value normally derived from a spherical top-hat collapse. Most of the methods utilizing this approach merely differ in the way they locate density peaks. The particle collector codes – above all the FOF method – connect and link particles together that are close to each other (either in a 3D configuration or in 6D phase space). They afterwards determine the centre of this mass aggregation.

After the initial selection has been made, most methods apply a pruning phase where gravitationally unbound particles are removed from the object. While this unbinding procedure is not essential for isolated field haloes, it is vital for subhaloes in order to properly alleviate the contamination by host halo particles. Furthermore, for subhaloes, it appears essential to define the first guess for bound particles upon a stable and reproducible criterion for the subhalo edge. One cannot extend the (spherical) shells out to the point where the density drops below some pre-selected multiple of the universal background density as this level will not be reached anymore; one needs to 'truncate' the object beforehand, usually at the point where the density rises again due to the fact that the subhalo is embedded within a host. Similarly, particle-collecting codes which use simple 'proximity' as a criterion for grouping particles need to adjust their yardsticks. However, the situation may be a bit more straightforward for 6D phase-space finders as we expect the velocity distributions of the host and the subhalo to be different.

Driven by the explosion of high-quality observational data, simulations of cosmological structure formation have moved to increasingly high mass and force resolution. The simulation codes and techniques have been continuously refined over the past few decades, providing us with methods that are akin yet different: they all have to solve the collisionless Boltzmann equation simultaneously with Poisson's equation and the equations that govern gas physics. In order to verify their credibility, the past few years have seen substantial efforts to intercompare the results stemming from these different techniques (cf. Frenk et al. 1999; Knebe et al. 2000; O'Shea et al. 2005; Agertz et al. 2007; Heitmann et al. 2008; Tasker et al. 2008). *However, to date, the literature lacks a quantitative comparison of the various halo-finding techniques.* While some efforts have been directed towards this goal (e.g. Lacey & Cole 1994; White 2002; Gill et al. 2004; Cohn & White 2008; Knollmann & Knebe 2009; Lukić et al. 2009; Maciejewski et al. 2009; Tweed et al. 2009), these studies primarily scratched the surface and no one has yet presented a conclusive intercomparison based upon a well-defined test suite. In addition, we would like to stress again that the analysis of massive state-of-the-art simulations is a non-trivial task, especially when it comes to the detailed substructure of the haloes. Furthermore, various definitions of the extent of a halo exist within the literature, making comparisons of the results from different groups far from straightforward (cf. White 2001; Lukić et al. 2009).

We though acknowledge that there is a body of the literature available that has compared halo-finder methods to theoretical predictions (e.g. Press & Schechter 1974; Lacey & Cole 1994; Sheth & Tormen 1999; Jenkins et al. 2001; Robertson et al. 2009; Courtin et al. 2011). While this is important work, it nevertheless rather

often leads to halo finders being tuned to match theoretical expectations than testing the validity of the code in the first place; the theories have sometimes been used to answer 'what halo definition is required to match theoretical expectations?' This may therefore mask important differences between a simple linear theory and the full non-linear growth of the structure in the Universe. In this paper, we focus instead on directly comparing different codes for halo finding and leave theoretical expectations aside.

In summary, there is no clear definition of 'what is a (dark) matter halo?' never mind 'what is a subhalo?' Workers in the field of simulation analysis tend to utilize their own definitions and codes to study the properties of haloes in cosmological simulations. This paper aims at rectifying this situation by presenting the first-ever coherent halo-finder comparison involving a substantial number of codes as well as providing the community with a well-defined set of test cases. However, we would like to caution the reader that the prime objective of this comparison is *codes* and not *algorithms*. Therefore, while certain codes may be based upon the same algorithm, they still may yield (marginally) different results due to the individual realization of that algorithm.

1.2 The workshop

During the last week of 2010 May, we held the workshop 'Haloes going MAD' in Miraflores de la Sierra close to Madrid, dedicated to the issues surrounding identifying haloes in cosmological simulations. Amongst other participants, 15 halo-finder representatives were present. The aim of this workshop was to define (and use!) a unique set of test scenarios for verifying the credibility and reliability of such programs. We applied each and every halo finder to our newly established suite of test cases and cross-compared the results.

To date most halo finders were introduced (if at all) in their respective code papers which presented their underlying principles and subjected them to tests within a full cosmological environment [primarily matching (sub)halo mass functions to theoretical models and fitting functions] and hence no general benchmarks such as the ones designed at the workshop and presented below existed prior to our meeting. Our newly devised suite of test cases is designed to be simple yet challenging enough to assist in establishing and gauging the credibility and functionality of all commonly employed halo finders. These tests include mock haloes with well-defined properties as well as a state-of-the-art cosmological simulation. They involve the identification of individual objects, various levels of substructure and dynamically evolving systems. The cosmological simulation has been provided at various resolution levels with the best resolved containing a sufficient number of particles (1024^3) that it can only presently be analysed in parallel.

All the test cases and the analysis presented here is publicly available from http://popia.ft.uam.es/HaloesGoingMAD under the tab 'The Data'.

1.3 How to compare haloes?

One of the most crucial questions to address is obviously 'how to define a halo?' This question is intimately related to 'how do we fairly cross-compare the results of the various halo finders?' While we all agreed that the proper definition of a halo should be a 'gravitationally bound object', how the size of a halo should be defined proved harder to agree upon. The 'virial radius' is not a well-defined property as its precise definition can (and does) vary

from halo finder to halo finder.[1] Furthermore, this quantity is ill-defined for subhaloes that live within the environment of a host halo. While there is some work available that allows for a conversion between commonly applied methods to calculate the mass of an isolated field halo (see e.g. White 2001; Lukić et al. 2009), such variations in definition will nevertheless lead to discrepancies in a cross-comparison and hence we decided to abandon the ambiguous definition for the edge of a halo and rather focus on a property that uniquely specifies the halo for the code-comparison project: the peak of the rotation curve as characterized by v_{max} and the radial location of this peak R_{max}. It has been argued (e.g. Ascasibar & Gottlöber 2008) that these quantities do indeed provide a physically motivated scale for DM haloes, showing that, in contrast to the inner regions, there is substantial scatter in their physical properties, as well as significant systematic trends with halo mass and cosmic epoch, beyond the radius R_{max}.

However, utilizing v_{max} raises two obvious issues: first, as v_{max} is reached quite close to the centre of the halo, its measurement is obviously sensitive to resolution. Secondly, as the value of v_{max} is set by the central particles, it is not very sensitive to tidal stripping. The relationship between R_{max} and R_{vir} for a range of NFW (Navarro et al. 1995, 1996, 1997) halo concentrations is given in fig. 6 of Muldrew, Pearce & Power (2011). The resolution issue can be addressed by increasing the number of particles required when studying subhalo properties so that v_{max} will always be resolved sufficiently and credibly. The relevance of the stripping issue though depends upon the questions to be asked of the simulation data – are we interested in a (stable) measure of the (original) infall mass of the subhalo or do we want to quantify the mass inside the tidal radius? For the comparison project, we decided to evaluate v_{max} in order to have a stable quantity. We further agreed that this quantity is better related to observational data as it is possible to observe rotation curves (and hence v_{max}), whereas the same ambiguity applies to observers: what is the (outer) edge of a halo and/or galaxy? Nevertheless, we also decided to include N_{part} (i.e. the total number of gravitationally bound particles as returned by the respective halo finder) in the comparison as a halo is (or should be) a gravitationally bound entity. The values for N_{part} are the ones directly returned by the halo finder and are based upon the internal criteria each code uses. How (and if) to perform the unbinding procedure and what particles to consider as belonging to the (sub)halo were questions left for each group taking part to answer as they saw fit. For several groups, these particle lists would normally be pruned further during an additional post-processing phase prior to obtaining halo properties. The numbers given here therefore serve solely as an indicator of whether or not particles are missing and/or – in case of subhaloes – belong to the host. In addition, we also used the list of particles belonging to each halo to calculate a fiducial M_{200} value [defined via $M(<r)/4\pi r^3 = 200 \times \rho_{crit}$] considering the object in isolation, even for subhaloes: there are physical situations – like the dynamical friction on infalling loose groups (e.g. Read et al. 2008; Lux, Read & Lake 2010) – where the (total) mass is the physically important quantity. Such examples of the limitation of the v_{max} value as a proxy for mass have also been witnessed in our test cases and we will come back to it in Section 4.1.3.

The first preliminary comparisons focusing on the spatial location, v_{max}, and the number of bound particles for the static mock

---

[1] We like to add the cautionary remark that a lot of the properties and in particular any 'radius' is based upon the assumption of spherical symmetry which is not valid for all halo finders presented here.

haloes indicate that even though there exist a variety of different approaches for halo finding, most of the codes agree with the known correct result well. If substructure is located close to the centre of the host halo, then all the codes tested experience some difficulties in accurately recovering it, with all the finders based in 3D configuration space missing some material. For subhaloes placed near the very centre of the host halo, the more sophisticated 6D finders based in phase space – while correctly noting the existence of a substructure – often overestimated the associated mass due to the confusion with the material in the host halo. After proving to ourselves that we could all successfully reproduce the location and scale of a supplied mock halo, we performed a resolution study where the mass and hence the number of particles in a subhalo was gradually lowered. We found that practically all halo finders have a completeness limit of 30–40 particles; substructure objects smaller than these are not reliably found. Once we had established a firm baseline for our comparisons, we extended the study to consider a full cosmological volume at varying resolution. The results of this comparison are presented in Section 4 below after we first briefly introduce each of the halo finders involved in the comparison project in Section 2 and describe the setup of our mock haloes in Section 3. Finally, we wrap up and present some conclusions in Section 5.

2 THE CODES

In this section, we are going to *briefly* present the codes that participated in the The Halo-Finder Comparison Project. We highlight their main features allowing for a better understanding of any (possible) differences in the comparison (Section 4). The prime information to be found in each code paragraph should be sufficient to understand how the algorithm works, how the initial particle content of a halo is obtained, the way the (sub)halo centre and edge are calculated, how the unbinding is performed and which method of parallelization has been applied. Note that not all halo finders perform an unbinding, are parallelized or suitable to detect subhaloes, and we explicitly stress that this section is neither intended as a review of all available halo finders nor intended as an elaborate exposition of the partaking codes; for the latter, we refer the reader to the respective code papers referenced in the subsection of each halo finder.

As much as possible, the halo finders have been organized in terms of their methodology: SO finders first followed by FOF-based finders with 6D phase-space finders last. This applies to both the presentation in this section and the comparison in Section 4.

2.1 AHF (Knollmann & Knebe)

The MPI+OpenMP parallelized halo finder AHF[2] (AMIGA Halo Finder, Knollmann & Knebe 2009) is an improvement of the MHF halo finder (Gill et al. 2004), which employs a recursively refined grid to locate local overdensities in the density field. The identified density peaks are then treated as centres of prospective haloes. The resulting grid hierarchy is further utilized to generate a halo tree readily containing the information which halo is a (prospective) host and subhalo, respectively. We therefore like to stress that our halo-finding algorithm is fully recursive, automatically identifying haloes, subhaloes, sub-subhaloes, etc. Halo properties are calculated based on the list of particles asserted to be gravitationally

bound to the respective density peak. To generate this list of particles, we employ an iterative procedure starting from an initial guess of particles. This initial guess is based again upon the adaptive grid hierarchy: for field haloes we start with considering all particles out to the isodensity contour encompassing the overdensity defined by the virial criterion based upon the spherical top-hat collapse model; for subhaloes, we gather particles up to the grid level shared with another prospective (sub)halo in the halo tree which corresponds to the upturn point of the density profile due to the embedding within a (background) host. This tentative particle list is then used in an iterative procedure to remove unbound particles: in each step of the iteration, all particles with a velocity exceeding the local escape velocity, as given by the potential based on the particle list at the start of the iteration, are removed. The process is repeated until no particles are removed anymore. At the end of this procedure, we are left with bona fide haloes defined by their bound particles and we can calculate their integral and profiled quantities.

The only parameter to be tuned is the refinement criterion used to generate the grid hierarchy that serves as the basis for the halo tree and also sets the accuracy with which the centres are being determined. The virial overdensity criterion applied to find the (field) halo edges is determined from the cosmological model of the data though it can readily be tailored to specific needs; for the analysis presented here, we used $200 \times \rho_{\text{crit}}$. For more details on the mode of operation and actual functionality, we refer the reader to the two code-description papers by Gill et al. (2004) and Knollmann & Knebe (2009), respectively.

2.2 ASOHF (Planelles & Quilis)

The ASOHF finder (Planelles & Quilis 2010) is based on the SO approach. Although it was originally created to be coupled to an Eulerian cosmological code, in its actual version, it is a stand-alone halo finder capable of analysing the outputs from cosmological simulations, including different components (i.e. DM, gas and stars). The algorithm takes advantage of an adaptive mesh refinement (AMR) scheme to create a hierarchy of nested grids placed at different levels of refinement. All the grids at a certain level, named patches, share the same numerical resolution. The higher the level of refinement, the better the numerical resolution, as the size of the numerical cells gets smaller. The refining criteria are open and can be chosen depending on the application. For a general purpose, ASOHF refines when the number of particles per cell exceeds a user-defined parameter. Once the refinement levels are set up, the algorithm applies the SO method independently at each of those levels. The parameters needed by the code are the following: (i) the cosmological parameters when analysing cosmological simulations; (ii) the size of the coarse cells, the maximum number of refinement levels (N_{levels}) and the maximum number of patches (N_{patch}) for all levels in order to build up the AMR hierarchy of nested grids; (iii) the number of particles per cell in order to choose the cells to be refined; and (iv) the minimum number of particles in a halo.

After this first step, the code naturally produces a tentative list of haloes of different sizes and masses. Moreover, a complete description of the substructure (haloes within haloes) is obtained by applying the same procedure on the different levels of refinement. A second step, not using the cells but the particles within each halo, makes a more accurate study of each of the previously identified haloes. These prospective haloes (subhaloes) may include particles which are not physically bound. In order to remove unbound particles, the local escape velocity is obtained at the position of each particle. To compute this velocity, we integrate Poisson equation

---

[2] AHF is freely available from http://www.popia.ft.uam.es/AMIGA

assuming spherical symmetry. If the velocity of a particle is higher than the escape velocity, the particle is assumed to be unbound and is therefore removed from the halo (subhalo) being considered. Following this procedure, unbound particles are removed iteratively along a list of radially ordered particles until no more of them need to be removed. In the case that the number of remaining particles is less than a given threshold, the halo is dropped from the list.

After this cleaning procedure, all the relevant quantities for the haloes (subhaloes) as well as their evolutionary merger trees are computed. The lists of (bound) particles are used to calculate canonical properties of haloes (subhaloes), like the position of the halo centre, which is given by the centre of mass of all the bound particles, and the size of the haloes, given by the distance of the farthest bound particle to the centre.

The ability of the ASOHF method to find haloes and their substructures is limited by the requirement that appropriate refinements of the computational grid exist with enough resolution to spot the structure being considered. In comparison to algorithms based on linking strategies, ASOHF does not require a linking length to be defined, although at a given level of refinement the size of the cell can be considered as the linking length of this particular resolution.

The version of the code used in this comparison is serial, although there is already a first parallel version based on OpenMP.

2.3 BDM (Klypin & Ceverino)

The BDM (Bound Density Maxima) halo finder originally described in Klypin & Holtzman (1997) uses a spherical 3D overdensity algorithm to identify haloes and subhaloes. It starts by finding the local density at each individual particle position. This density is defined using a top-hat filter with a constant number of particles, N_{filter}, which typically is $N_{\text{filter}} = 20$. The code finds all maxima of density, and for each maximum it finds a sphere containing a given overdensity mass $M_\Delta = (4\pi/3)\Delta\rho_{\text{cr}}R_\Delta^3$, where ρ_{cr} is the critical density and Δ is the specified overdensity.

For the identification of distinct haloes, the code uses the density maxima as halo centres; amongst overlapping spheres the code finds the one that has the deepest gravitational potential. Haloes are ranked by their (preliminary) size, and their final radius and mass are derived by a procedure that guarantees the smooth transition of properties of small haloes when they fall into a larger host halo becoming subhaloes: this procedure assigns either R_Δ or R_{dist} as the radius for a currently infalling halo, depending on the environmental conditions, where R_{dist} measures the distance of the infalling halo from the surface of the soon-to-be host halo.

The identification of subhaloes is a more complicated procedure: centres of subhaloes are certainly density maxima, but not all density maxima are centres of subhaloes. BDM eliminates all density maxima from the list of subhalo candidates which have less than N_{filter} self-bound particles. For the remaining set of prospective subhaloes, the radii are determined as the minimum of the following three distances: (i) the distance from the nearest barrier point [i.e. centres of previously defined (sub)haloes]; (ii) the distance from its most remote bound particle; and (iii) the truncation radius (i.e. the radius at which the average density of bound particles has an inflection point). This evaluation involves an iterative procedure for removing unbound particles and starts with the largest density maximum.

The unbinding procedure requires the evaluation of the gravitational potential which is found by first finding the mass in spherical shells and then by integration of the mass profile. The binning is done in log radius with a very small bin size of $\Delta\log(R) = 0.005$.

The bulk velocity of either a distinct halo or a subhalo is defined as the average velocity of the 30 most bound particles of that halo or of all particles, if the number of particles is less than 30. The number 30 is a compromise between the desire to use only the central (sub)halo region for the bulk velocity and the noise level.

The code uses a domain decomposition for MPI parallelization and OpenMP for the parallelization inside each domain.

2.4 PSO (Sutter & Ricker)

The PSO (parallel spherical overdensity) halo finder is a fast, highly scalable MPI-parallelized tool directly integrated into the FLASH simulation code that is designed to provide on-the-fly halo finding for use in subgrid modelling, merger tree analysis and AMR schemes (Sutter & Ricker 2010). The PSO algorithm identifies haloes by growing SO spheres. There are four adjustable parameters controlling the desired overdensity criteria for centre detection and halo size, the minimum allowed halo size, and the resolution of the halo radii relative to the grid resolution. The algorithm discovers halo centres by mapping DM particles on to the simulation mesh and selecting cell centres where the cell density is greater than the given overdensity criterion. The algorithm then determines the halo edge using the SO radius by collecting particles using the FLASH AMR tree hierarchy. The algorithm determines the halo centre, bulk velocity, mass and velocity dispersion without additional post-processing. PSO is provided both as an API for use in-code and as a stand-alone halo finder.

2.5 LANL (Lukić, Fasel & Hsu)

The LANL halo finder is developed to provide on-the-fly halo analysis for simulations utilizing hundreds of billions of particles and is integrated into the MC^3 code (Habib et al. 2009), although it can also be used as a stand-alone halo finder. Its core is a fast kD-tree FOF halo finder which uses 3D (block), structured decomposition to minimize the surface-to-volume ratio of the domain assigned to each process. As it is aimed at large-scale structure simulations (100+ Mpc h^{-1} on the side), where the size of any single halo is much smaller than the size of the whole box, it uses the concept of 'ghost zones' such that each process gets all the particles inside its domain as well as those particles which are around the domain within a given distance (the overload size, a code parameter chosen to be larger than the size of the biggest halo we expect in the simulation). After each process runs its serial version of a FOF finder, MPI-based 'halo stitching' is performed to ensure that every halo is accounted for, and accounted for only once.

If desired, spherical 'SO' halo properties can be found using the FOF haloes as a proxy. Those SO haloes are centred at the particle with the lowest gravitational potential, while the edge is at R_Δ – the radius enclosing an overdensity of Δ. It is well known that percolation-based FOF haloes suffer from the overbridging problem; therefore, if we want to ensure the completeness of our SO sample, then we should run the FOF algorithm with a smaller linking length than usual in order to capture all density peaks, but still avoid overbridging at the scale of interest (which depends on our choice of Δ). Overlapping SO haloes are permitted, but the centre of one halo may not reside inside another SO halo (that would be considered as a substructure, rather than a 'main' halo). The physical code parameters are the linking length for the FOF haloes and overdensity parameter Δ for SO haloes. Technical parameters are the overload size and the minimum number of particles in a halo.

The LANL halo finder is being included in the standard distributions of the PARAVIEW[3] package, enabling researchers to combine the analysis and visualization of their simulations. A substructure finder is currently under development.

2.6 SUBFIND (Iannuzzi, Springel & Dolag)

SUBFIND (Springel et al. 2001a) identifies gravitationally bound, locally overdense regions within an input parent halo, traditionally provided by a FOF group finder, although other group finders could be used in principle as well. The densities are estimated based on the initial set of all particles via adaptive kernel interpolation based on a number N_{dens} of smoothing neighbours. For each particle, the nearest N_{ngb} neighbours are then considered for identifying local overdensities through a topological approach that searches for saddle points in the isodensity contours within the global field of the halo. This is done in a top-down fashion, starting from the particle with the highest associated density and adding particles with progressively lower densities in turn. If a particle has only denser neighbours in a single structure, then it is added to this region. If it is isolated, then it grows a new density peak, and if it has denser neighbours from two different structures, an isodensity contour that traverses a saddle point is identified. In the latter case, the two involved structures are joined and registered as candidate subhaloes if they contain at least N_{ngb} particles. These candidates, selected according to the spatial distribution of particles only, are later processed for gravitational self-boundness. Particles with positive total energy are iteratively dismissed until only bound particles remain. The gravitational potential is computed with a tree algorithm, such that large haloes can be processed efficiently. If the number of the remaining bound number of particles is at least N_{ngb}, then the candidate is ultimately recorded as a subhalo. The set of initial substructure candidates forms a nested hierarchy that is processed inside out, allowing the detection of substructures within substructures. However, a given particle may only become a member of one substructure, that is, SUBFIND decomposes the initial group into a set of disjoint self-bound structures. Particles not bound to any genuine substructure are assigned to the 'background halo'. This component is also checked for self-boundness, so that some particles that are not bound to any of the structures may remain. For all substructures as well as the main halo, the particle with the minimum gravitational potential is adopted as (sub)halo centre. For the main halo, SUBFIND additionally calculates a SO virial mass around this centre, taking into account all particles in the simulation (i.e. not just those in the FOF group that are analysed). There exist both serial and MPI-parallelized versions of SUBFIND, which implement the same underlying algorithm. For more details, we refer the reader to the paper by Springel et al. (2001a).

2.7 FOF (Gottlöber & Turchaninov)

In order to analyse large cosmological simulations with up to 2048^3 particles, we have developed a new MPI version of the hierarchical FOF algorithm with low memory requests. It allows us to construct very fast clusters of particles at any overdensity (represented by the linking length) and to deduce the progenitor–descendant relationship for clusters in any two different time-steps. The particles in a simulation can consist of different species (DM, gas, stars) of different mass. We consider them as an undirected graph with

positive weights, namely the lengths of the segments of this graph. For simplicity, we assume that all weights are different. Then, one can show that a unique minimal spanning tree (MST) of the point distribution exists, namely the shortest graph which connects all points. If subgraphs cover the graph, then the MST of the graph belongs to the union of MSTs of the subgraphs. Thus, subgraphs can be constructed in parallel. Moreover, the geometrical features of the clusters, namely the fact that they occupy mainly almost non-overlapping volumes, allow the construction of fast parallel algorithms. If the MST has been constructed, all possible clusters at all linking lengths can be easily determined. To represent the output data, we apply topological sorting to the set of clusters which results in a cluster-ordered sequence. Every cluster at any linking length is a segment of this sequence. It contains the distances between adjacent clusters. Note that for the given MST there exist many cluster-ordered sequences which differ in the order of the clusters but yield the same set of clusters at a desired linking length. If the set of particle clusters has been constructed, further properties (centre of mass, velocity, shape, angular momentum, orientation, etc.) can be directly calculated. Since this concept is by construction aspherical, a circular velocity (as used to characterize objects found with SO algorithms) cannot be determined here. The progenitor–descendant relationship is calculated for the complete set of particles by comparison of the cluster-ordered sequences at two different output times.

The hierarchical FOF algorithm identifies objects at different overdensities depending on the chosen linking length (More et al. 2011). In order to avoid artificial misidentifications of subhaloes on high overdensities, one can add an additional criterion. Here we have chosen the requirement that the spin parameter of the subhalo should be smaller than one. All subhaloes have been identified at 512 times the virial overdensity. Thus, only the highest density peak has been taken into account for the mass determination and the size of the object, which are therefore underestimated. The velocity of the density peak is estimated correctly but without removing unbound particles.

2.8 PFOF (Rasera & Roy)

PFOF (Parallel FOF) is a MPI-based parallel FOF halo finder which is used within the DEUS Consortium[4] at the Laboratory Universe and Theories. It has been parallelized by Roy and was used in several studies involving large N-body simulations such as Courtin et al. (2011) and Rasera et al. (2010). The principle is the following: first, particles are distributed in cubic subvolumes of the simulation and each processor deals with one 'cube' and runs the FOF algorithm locally. Then, if a structure is located close to the edge of a cube, PFOF checks if there are particles belonging to the same halo in the neighbouring cube. This process is carried out iteratively until all haloes extending across multiple cubes have been merged. Finally, particles are sorted on a per halo basis, and the code writes two kinds of output: particles sorted per region and particles sorted per halo. This makes any post-processing straightforward because each halo or region can be analysed individually on a single CPU server. PFOF was successfully tested on up to 4096 Bluegene/P cores with a 2048^3 particle N-body simulation. In this paper, the serial version was used for mock haloes and small cosmological simulations, and the parallel version for larger runs. The linking length was set to $b = 0.2$ (however, see Courtin et al. 2011, for a discussion on the

halo definition) and the minimum halo mass to 100 particles; the halo centres reported here are the centre of mass of the respective particle distribution.

2.9 Ntropy-fofsv (Gardner, McBride & Stinson)

The Ntropy parallel programming framework is derived from *N*-body codes to help address a broad range of astrophysical problems.[5] This includes an implementation of a simple but efficient FOF halo finder, Ntropy-fofsv, which is more fully described in Gardner et al. (2007a) and Gardner et al. (2007b). Ntropy provides a 'distributed shared memory' implementation of a *k*D-tree, where the application developer can reference tree nodes as if they exist in a global address space, even though they are physically distributed across many compute nodes. Ntropy uses the *k*D-tree data structures to speed up the FOF distance searches. It also employs an implementation of the Shiloach & Vishkin (1982) parallel connectivity algorithm to link together the haloes that span separate processor domains. The advantage of this method is that no single computer node requires the knowledge of all of the groups in the simulation volume, meaning that Ntropy-fofsv is scalable to petascale platforms and handles large data input. This algorithm was used in the mock halo test cases to stitch together particle groups found across many threads into the one main FOF halo. As FOF is a deterministic algorithm, Ntropy-fofsv takes a single physical linking length to group particles into FOF haloes without performing any particle unbinding or subhalo identification. The halo centres for the analysis presented here use centre-of-mass estimates based on the FOF particle list. Ntropy achieves parallelization by calling the 'machine-dependent library' that consists of high-level operations such as 'acquire_treenode' or 'acquire_particle'. This library is rewritten for a variety of models (MPI, POSIX Threads, Cray SHMEM, etc.), allowing the framework to extract the best performance from any parallel architecture on which it is run.

2.10 voboz (Neyrinck)

Conceptually, a voboz (VOronoi BOund Zones, Neyrinck et al. 2005) halo or subhalo is a density peak surrounded by gravitationally bound particles that are down steepest density gradients from the peak. A statistical significance is measured for each (sub)halo, based on the probability that Poisson noise would produce it.

The only physical parameter in voboz is the density threshold characterizing the edge of (parent) haloes (set to 200 times the mean density here), which typically only affects their measured masses. To return a definite halo catalogue, we also impose a statistical-significance threshold (set to 4σ here), although depending on the goal of a study, this may not be necessary.

Density peaks are found using a Voronoi tessellation (parallelizable by splitting up the volume), which gives an adaptive, parameter-free estimate of each particle's density and a set of neighbours (e.g. Schaap & van de Weygaert 2000). Each particle is joined to the peak particle (whose position is returned as the halo centre) that lies up the steepest density gradient from that particle. A halo associated with a high-density peak will also contain smaller density peaks. The significance of a halo is judged according to the ratio of its central density to a saddle point joining the halo to a halo with a higher central density, comparing to a Poisson point process. Pre-unbinding (sub)halo boundaries are defined along these density ridges.

Unbinding evaporates many spurious haloes and often brings other halo boundaries inwards a bit, reducing the dependence on the outer density contrast. Particles not gravitationally bound to each halo are removed iteratively, by comparing their potential energies (measured as sums over all other particles) to kinetic energies with respect to the velocity centroid of the halo's core (i.e. the particles that directly jump up density gradients to the peak). The unbinding is parallelized using OpenMP. In the cosmological test, we remove haloes with fewer than 20 particles from the voboz halo list.

2.11 origami (Falck, Neyrinck & Aragon-Calvo)

origami (Order-ReversIng Gravity Apprehended Mangling Indices, Falck et al., in preparation) uses a natural, parameter-free definition of the boundary between haloes and the non-halo environment around them: halo particles are particles that have experienced shell-crossing. This dynamical definition does not make use of the density field, in which the boundary can be quite ambiguous. In 1D, shell-crossings can be detected by looking for pairs of particles whose positions are out-of-order compared with their initial positions. In 3D, then, a halo particle is defined as a particle that has undergone shell-crossings along three orthogonal axes. Similarly, this would be two axes for a filament, one for a wall and zero for a void. There is a huge number of possible sets of orthogonal axes in the initial grid to use to test for shell-crossing, but we only used four simple ones, which typically suffice to catch all the shell-crossings. We used the Cartesian *x*-, *y*- and *z*-axes, as well as the three sets of axes consisting of one Cartesian axis and two (45°) diagonal axes in the plane perpendicular to it.

Once halo particles have been tagged, there are many possible ways of grouping them into haloes. For this paper, we grouped them on a Voronoi tessellation of final-conditions particle positions. This gives a natural density estimate [e.g. Schaap & van de Weygaert 2000; Voronoi Tessellation Field Estimator (VTFE)] and a set of neighbours for each particle. Haloes are sets of halo particles connected to each other on the Voronoi tessellation. To prevent haloes from being unduly linked, we additionally require that a halo contains at most one halo 'core', defined as a set of particles connected on the tessellation that all exceed a VTFE density threshold. This density threshold is the only parameter in our algorithm, since the initial tagging of halo particles is parameter-free; for this study, we set it to 200 times the mean density. We partition connected groups of halo particles with multiple cores into haloes as follows: each core iteratively collects particles in concentric rings of Voronoi neighbours until all halo particles are associated. The tagging procedure establishes halo boundaries, so no unbinding procedure is necessary. Also, we note that, currently, the algorithm does not identify subhaloes. We remove haloes with fewer than 20 particles from the origami halo catalogue, and the halo centre reported is the position of the halo's highest density particle.

Note that due to its nature origami *is only applicable to cosmological simulations and hence only enters the comparison project in the respective Section 4.2.*

2.12 skid (Stadel & Potter)

skid (Spline Kernel Interpolative Denmax),[6] first mentioned in Governato et al. (1997) and extensively described in Stadel (2001),

---

[5] http://www.phys.washington.edu/users/gardnerj/ntropy

[6] The OpenMP parallelized version of skid can be freely downloaded from http://www.hpcforge.org

finds density peaks within N-body simulations and subsequently determines all associated bound particles, thereby identifying haloes. It is important to stress that SKID will only find the smallest scale haloes within a hierarchy of haloes as is generally seen in cosmological structure formation simulations. Unlike original DENMAX (Bertschinger & Gelb 1991; Gelb 1992) which used a fixed grid based density estimator, SKID uses smoothed particle hydrodynamics (SPH) kernel averaged densities which are much better suited to the Lagrangian nature of N-body simulations and allow the method to locally adapt to the large dynamic range found in cosmological simulations.

Particles are slowly slid (each step moving the particles by a distance of the order of the softening length in the simulation) along the local density gradient until they pool at a maximum, each pool corresponding to each initial group. This first phase of SKID can be computationally very expensive for large simulations, but is also quite robust.

Each pool is then 'unbound' by iteratively evaluating the binding energy of every particle in their original positions and then removing the most non-bound particle until only bound particles remain. This removes all particles that are not part of substructure either because they are part of larger scale structure or because they are part of the background.

SKID can also identify structure composed of gas and stars in hydrodynamical simulations using the DM only for its gravitational binding effect. The 'Haloes going MAD' meeting has motivated the development of an improved version of the algorithm capable of also running on parallel computers.

2.13 ADAPTAHOP (Tweed & Colombi)

The code ADAPTAHOP is described in appendix A of Aubert et al. (2004). The first step is to compute an SPH density for each particle from the 20 closest neighbours. Isolated haloes are then described as groups of particles above a density threshold ρ_t, where this parameter is set to 80, which closely matches results of a FOF group finder with parameter $b = 0.2$. To identify subhaloes within those groups, local density maxima and saddle points are detected. Then, by increasing the density threshold, it is a simple matter to decompose haloes into nodes that are either density maxima or groups of particles whose density is between two values of saddle points. A node structure tree is then created to detail the whole structure of the halo itself. Each leaf of this tree is a local density maximum and can be interpreted as a subhalo. However, further post-processing is needed to define the halo structure tree, describing the host halo itself, its subhaloes and subhaloes within subhaloes. This part of the code is detailed in Tweed et al. (2009); the halo structure tree is constructed so that the halo itself contains the most massive local maximum (Most massive Sub maxima Method, MSM). This method gives the best result for isolated snapshots, as used in this paper.

In more detail, ADAPTAHOP needs a set of seven parameters. The first parameter is the number of neighbours n_{nei} used with a kD-tree scheme in order to estimate the SPH density. Among these n_{nei} neighbours, the n_{hop} closest are used to sweep through the density field and detect both density maxima and saddle points. As previously mentioned, the parameter ρ_t sets the halo boundary. The decomposition of the halo itself into leaves that are to be redefined as subhaloes has to fulfil certain criteria set by the remaining four parameters. The most relevant is the statistical significance threshold, set via the parameter *fudge*, defined via $(\langle \rho \rangle - \rho_t)/\rho_t > fudge/\sqrt{N}$, where N is the number of particles in the leaves. The minimal mass

of a halo is limited by the parameter $n_{members}$, the minimum number of particles in a halo. Any potential subhalo has also to respect two conditions with respect to the density profile and the minimal radius, through the parameters α and f_ϵ. These two values ensure that a subhalo has a maximal density ρ_{max} such as $\rho_{max} > \alpha \langle \rho \rangle$ and a radius greater than f_ϵ times the mean interparticle distance. We used the following set of parameters ($n_{nei} = n_{hop} = 20$, $\rho_t = 80$, *fudge* $= 4$, $\alpha = 1$, $f_\epsilon = 0.05$ and $n_{members} = 20$). It is important to understand that all nodes are treated as leaves and must comply with aforementioned criteria before being further decomposed into separate structures. As for defining haloes and subhaloes themselves, this is done by grouping linked lists of particles corresponding to different nodes and leaves from the node structure tree. Further, the halo and subhalo centres are defined as the positions of the particle with the highest density. The halo edge corresponds to the ρ_t density threshold, whereas the saddle points define the subhalo edge.

Note that ADAPTAHOP is a mere topological code that does *not* feature an unbinding procedure. For substructures (whose boundaries are chosen from the saddle point value), this may have impact on the estimate of the mass as well as lead to the contamination by host particles.

2.14 HOT (Ascasibar)

This algorithm, still under development, computes the Hierarchical Overdensity Tree (HOT; Ascasibar, in preparation) of a point distribution in an arbitrary multidimensional space. HOT is introduced as an alternative to the MST for spaces where a metric is not well defined, like the phase space of particle positions and velocities.

The method is based on the Field Estimator for Arbitrary Spaces (FIESTAS, Ascasibar & Binney 2005). First, the space is tessellated 1D at a time, until it is divided into a set of hypercubical cells containing exactly one particle. Particles in adjacent cells are considered as neighbours. Then, the mass of each point is distributed over an adaptive smoothing kernel as described in Ascasibar (in preparation), which provides a key step in order to define a metric.

In the HOT+FIESTAS scheme, objects correspond to the peaks of the density field, and their boundaries are set by the isodensity contours at the saddle points. At each saddle point, the object containing less particles is attached to the most massive one, which may then be incorporated into even more massive objects in the hierarchy. This idea can be implemented by computing the MST of the data distribution, defining the distance between two neighbouring particles as the minimum density along an edge connecting them (i.e. the smallest of the two densities, or the density of the saddle point when it exists). However, this is not practical for two reasons. First, defining a path between two particles is not trivial when a metric is not available. Secondly, finding the saddle points would require a minimization along the path, which is extremely time-consuming when a large number of particles are involved. These problems may be overcome if the distance between two data points is given by the average density within the hyperbox they define.

Once the distances are defined in this way, HOT+FIESTAS computes the MST of the data distribution by means of Kruskal's algorithm (Kruskal 1956). The output of the algorithm consists of the tree structure, given by the parent of each data point in HOT, and a catalogue containing an estimate of the centroid (given by the density-weighted centre of mass) as well as the number of particles in the object (both including and excluding substructures). In order to discard spurious density fluctuations, a minimum number of points and density contrast are required for an object to be output to the catalogue. Currently, these parameters are set to

$N > 20$ particles and a contrast threshold $\rho_{\text{peak}}/\rho_{\text{background}} > 5$. Although these values seem to yield reasonable results, more experimentation is clearly needed.

In this work, the algorithm is applied to the particle positions only (HOT3D) as well as the full set of phase-space coordinates (HOT6D). Since it is intended as a general data analysis tool, not particularly optimized for the problem of halo identification, it should not (and does not) take into account any problem-specific knowledge such as the concepts of binding energy or virial radius. The latter quantity, as well as the maximum circular velocity, has been computed from the raw particle IDs returned by the code.

The definition of object boundaries in terms of the saddle points of the density field will have a relatively mild impact on the results concerning the mock haloes, but it is extremely important in the cosmological case. HOT+FIESTAS will, for instance, identify large-scale filamentary structures that are not considered haloes by any of the other algorithms (although many of these objects are indeed gravitationally bound).

On the other hand, keeping unbound particles will be an issue for subhaloes close to the centre of their host, especially in 3D, and a post-processing[7] script will be developed to perform this task.

Note that due to its present implementation HOT *is not yet applicable to cosmological simulations and hence only enters the comparison project in the mock halo Section 4.1.*

2.15 HSF (Maciejewski)

HSF (Hierarchical Structure Finder, Maciejewski et al. 2009) identifies objects as connected self-bound particle sets above some density threshold. This method consists of two steps. Each particle is first linked to a local DM phase-space density maximum by following the gradient of a particle-based estimate of the underlying DM phase-space density field. The particle set attached to a given maximum defines a candidate structure. In a second step, particles which are gravitationally unbound to the structure are discarded until a fully self-bound final object is obtained.

In the initial step, the phase-space density and phase-space gradients are estimated by using a 6D SPH smoothing kernel with a local adaptive metric as implemented in the ENBID code (Sharma & Steinmetz 2006). For the SPH kernel, we use N_{sph} between 20 and 64 neighbours, whereas for the gradient estimate, we use $N_{\text{ngb}} = 20$ neighbours.

Once phase-space densities have been calculated, we sort the particles according to their density in descending order. Then, we start to grow structures from high to low phase-space densities. While walking down in density we mark for each particle the two closest (according to the local phase-space metric) neighbours with higher phase-space density, if such particles exist. In this way, we grow disjoint structures until we encounter a saddle point, which can be identified by observing the two marked particles and seeing if they belong to different structures. A saddle point occurs at the border of two structures. According to each structure mass, all the particles below this saddle point can be attached to only one of the structures if it is significantly more massive than the other one, or redistributed between both structures if they have comparable masses. This is controlled by a simple but robust cut or grow criterion depending on a *connectivity parameter* α which is ranging from 0.2 up to 1.0. In addition, we test on each saddle point if structures are statistically significant when compared to Poisson noise

(controlled by a β parameter). At the end of this process, we obtain a hierarchical tree of structures.

In the last step, we check each structure against an unbinding criterion. Once we have marked its more massive partner for each structure, we sort them recursively such that the larger partners (parents) are always after the smaller ones (children). Then, we unbind structure after structure from children to parents and add unbound particles to the larger partner. If the structure has less than $N_{\text{cut}} = 20$ particles after the unbinding process, then we mark it as not bound and attach all its particles to its more massive partner (note that a smaller N_{cut} is used for the resolution study in Section 4.1.4). The most bound particle of each halo/subhalo defines its position centre.

Although HSF can be used on the entire volume, to speed up the process of the identification of the structures in the cosmological simulation volume, we first apply the FOF method to disjoint the particles into smaller FOF groups.

2.16 6DFOF (Zemp & Diemand)

6DFOF is a simple extension of the well-known FOF method which also includes a proximity condition in velocity space. Since the centres of all resolved haloes and subhaloes reach a similar peak phase-space density, they can all be found at once with 6DFOF. The algorithm was first presented in Diemand et al. (2006). The 6DFOF algorithm links two particles if the condition

$$\frac{(\boldsymbol{x}_1 - \boldsymbol{x}_2)^2}{\Delta x^2} + \frac{(\boldsymbol{v}_1 - \boldsymbol{v}_2)^2}{\Delta v^2} < 1 \tag{1}$$

is fulfilled. There are three free parameters: Δx, the linking length in position space, Δv, the linking length in velocity space, and N_{min}, the minimum number of particles in a linked group so that it will be accepted. For $\Delta v \to \infty$, it reduces to the standard FOF scheme. The 6DFOF algorithm is used for finding the phase-space coordinates of the high phase-space density cores of haloes on all levels of the hierarchy and is fully integrated in parallel within the MPI and OpenMP parallelized code PKDGRAV (Stadel 2001).

The centre position and velocity of a halo are then determined from the linked particles of that halo. For the centre position of a halo, one can choose between the following three types: (i) the centre of mass of its linked particles; (ii) the position of the particle with the largest absolute value of the potential among its linked particles; or (iii) the position of the particle which has the largest local mass density among its linked particles. For the analysis presented here, we chose type (iii) as our halo centre position definition. The centre velocity of a halo is calculated as the centre-of-mass velocity of its linked particles. Since in 6DFOF only the particles with a high phase-space density in the very centre of each halo (or subhalo) are linked together, it explains the somewhat different halo velocities (compared to the other halo finders) and slightly offset centres in cases where only a few particles were linked.

Other properties of interest (e.g. mass, size or maximum of the circular velocity curve) and the hierarchy level of the individual haloes are then determined by a separate profiling routine in a post-processing step. For example, a characteristic size and mass-scale definition (e.g. $r_{200\text{c}}$ and $M_{200\text{c}}$) for field haloes based on traditional SO criteria can be specified by the user. For subhaloes, a truncation scale can be estimated as the location where the mass density profile reaches a user-specified slope. During the profiling step, no unbinding procedure is performed. Hence, the profiling step does not base its (sub)halo properties upon particle lists but rather on

---

[7] HOT3D does not even read particle velocities.

spherical density profiles. Therefore, 6DFOF directly returned halo properties instead of the (requested) particle ID lists.

2.17 ROCKSTAR (Behroozi)

ROCKSTAR is a new phase-space-based halo finder designed to maximize halo consistency across time-steps; as such, it is especially useful for studying merger trees and halo evolution (Behroozi et al., in preparation). ROCKSTAR first selects particle groups with a 3D FOF variant with a very large linking length ($b = 0.28$). For each main FOF group, ROCKSTAR builds a hierarchy of FOF subgroups in phase space by progressively and adaptively reducing the linking length, so that a tunable fraction (70 per cent, for this analysis) of particles are captured at each subgroup as compared to the immediate parent group. For each subgroup, the phase-space metric is renormalized by the standard deviations of the particle position and velocity, that is, for two particles p_1 and p_2 in a given subgroup, the distance metric is defined as

$$d(p_1, p_2) = \left[\frac{(\boldsymbol{x}_1 - \boldsymbol{x}_2)^2}{\sigma_x^2} + \frac{(\boldsymbol{v}_1 - \boldsymbol{v}_2)^2}{\sigma_v^2} \right]^{1/2}, \qquad (2)$$

where σ_x and σ_v are the particle position and velocity dispersion, respectively, for the given subgroup. This metric ensures an adaptive selection of overdensities at each successive level of the FOF hierarchy.

When this is complete, ROCKSTAR converts FOF subgroups into haloes beginning at the deepest level of the hierarchy. For a subgroup without any further sublevels, all the particles are assigned to a single seed halo. If the parent group has no other subgroups, then all the particles in the parent group are assigned to the same seed halo as the subgroup. However, if the parent group has multiple subgroups, then particles are assigned to the subgroups' seed haloes based on their phase-space proximity. In this case, the phase-space metric is set by halo properties, so that the distance between a halo h and a particle p is defined as

$$d(h, p) = \left[\frac{(\boldsymbol{x}_h - \boldsymbol{x}_p)^2}{r_{\mathrm{vir}}^2} + \frac{(\boldsymbol{v}_h - \boldsymbol{v}_p)^2}{\sigma_v^2} \right]^{1/2}, \qquad (3)$$

where r_{vir} is the current virial radius of the seed halo and σ_v is the current particle velocity dispersion. This process is repeated at all levels of the hierarchy until all particles in the base FOF group have been assigned to haloes. Unbinding is performed using the full particle potentials (calculated using a modified Barnes & Hut method, Barnes & Hut 1986); halo centres are defined by averaging particle positions at the FOF hierarchy level which yields the minimum estimated Poisson error – which in practice amounts to averaging positions in a small region close to the phase-space density peak. For further details about the unbinding process and for details about the accurate calculation of halo properties, see Behroozi et al. (in preparation).

ROCKSTAR is a massively parallel code (hybrid OpenMP/MPI style); it can already run on up to 10^5 CPUs and on the very largest simulations ($>10^{10}$ particles). Additionally, it is very efficient, requiring only 56 bytes of memory per particle and 4–8 (total) CPU hours per billion particles in a simulation snapshot. The code is in the final stages of development; as such, the results in this paper are a minimum threshold for the performance and accuracy of the final version.[8]

[8] Those interested in obtaining a copy of the code as well as a draft of the paper should contact the author at behroozi@stanford.edu. The current acceptable input formats for simulation files are ART, GADGET-2 and ASCII.

3 THE DATA

In order to study, quantify and assess the differences between various halo-finding techniques, we, first, have to define a unique set of test cases. In that regard, we decided to split the suite of comparisons into two major parts:

(i) well-defined mock haloes consisting of field haloes in isolation as well as (sub-)subhaloes embedded within the density background of larger entities; and

(ii) a state-of-the-art cosmological simulation primarily focusing on the large-scale structure.

We further restricted ourselves to analysing DM-only data sets as the inclusion of baryons (especially gas and its additional physics) will most certainly complicate the issue of halo finding. As most of the codes participating in this comparison project do not consider gas physics in the process of object identification, we settled for postponing such a comparison to a later study.

We further adopted the following strategy for the comparison. For the mock haloes, each code was asked to return a list of particles and the centre of the (sub)halo as derived from applying the halo finder to the respective data set. These centres and particle lists were then post-processed by one single code deriving all the quantities studied below. By this approach we aimed at homogenizing the comparison and eliminating subtle code-to-code variations during the analysis process. However, we also need to acknowledge that not all codes complied with this request as they were not designed to return particle lists; those codes nevertheless provided the halo properties in question and are included in the comparison.

For the comparison of the cosmological simulations, each code merely had to return those halo properties to be studied, based upon each and every code individually. The idea was to compare the actual performance of the codes in a realistic setup without interference in the identification/analysis process.

3.1 Mock haloes

In order to be able to best quantify any differences in the results returned by different halo finders, it is best to construct test scenarios for which the correct answer is known in advance. Even though we primarily aim at comparing v_{max} and the number of gravitationally bound particles, we also want to have full control over various definitions of, for instance, virial mass, that is, we require haloes whose density profile is well known. Additionally, as subhalo detection is of prime interest in state-of-the-art cosmological simulations, we also place haloes within haloes within haloes, and so on. Further, sampling a given density profile with particles also gives us the flexibility to study resolution effects related to the number of particles actually used.

We primarily used the functional form for the (DM) density profile of haloes originally proposed in a series of papers by Navarro, Frenk & White (Navarro et al. 1995, 1996, 1997), the so-called 'NFW profile':

$$\frac{\rho(r)}{\rho_{\mathrm{crit}}} = \frac{\delta_{\mathrm{c}}}{r/r_{\mathrm{s}}(1 + r/r_{\mathrm{s}})^2}, \qquad (4)$$

where ρ_{crit} is the critical density of the universe, r_{s} is the scale radius and δ_{c} is the characteristic density. NFW haloes are characterized by their mass for a given enclosed overdensity,

$$M_\Delta = \frac{4\pi}{3} r_\Delta^3 \Delta \rho_{\mathrm{crit}}, \qquad (5)$$

where Δ is a multiple of the critical density that defines the magnitude of the overdensity and r_Δ is the radius at which this occurs.

Table 1. The properties of the (sub)haloes for the study of recovered halo properties presented in Sections 4.1.1 and 4.1.2. The number of particles $N_{\rm xxx}$ counts all particles out to $R_{\rm xxx}$ where the density drops below xxx $\times \rho_{\rm crit}$. Masses are given in $h^{-1}\,{\rm M_\odot}$, radii in h^{-1} kpc and velocities in km s^{-1}. Note that all haloes have been sampled out to $2 \times R_{100}$ and that the Plummer sub-subhalo does not reach this overdensity and has been truncated at 23.9 h^{-1} kpc. The halo type indicates whether the halo is a host, a subhalo or a sub-subhalo. $R_{\rm s}$ is the scalelength of the appropriate halo type.

Profile	Type	N_{100}	M_{100}	R_{100}	N_{200}	M_{200}	R_{200}	$R_{\rm s}$	$v_{\rm max}$
NFW	Host	10^6	10^{14}	947.4	760 892	7.61×10^{13}	689.1	189.5	715
	Sub	10^4	10^{12}	204.1	8066	8.07×10^{11}	151.4	17.0	182
	Sub-sub	10^2	10^{10}	44.0	84	8.42×10^9	33.1	2.6	43
Plummer	Host	10^6	10^{14}	947.0	966 326	9.66×10^{13}	760.5	190.0	961
	Sub	10^4	10^{12}	204.0	9937	9.94×10^{11}	161.7	17.0	314
	Sub-sub	10^2	10^{10}	23.9	100	10.00×10^9	23.9	2.6	79

The characteristic density is then defined as

$$\delta_{\rm c} = \frac{\Delta}{3} \frac{c^3}{\ln(1+c) - c/(1+c)}, \tag{6}$$

where $c = r_\Delta/r_{\rm s}$ is the concentration. The mock haloes were generated by using a predefined number of particles that reproduced the NFW profile even though the consensus has moved away from the statement that DM haloes follow this particular profile all the way down to the centre. We are not interested in probing those very central regions where the density profile starts to deviate from the NFW form as found nowadays in cosmological simulations (Stadel et al. 2009; Navarro et al. 2010). We need to stress that the position and size of the maximum of the rotation curve is in fact unaffected in all tests presented here. The velocities of the particles were then assigned using the velocity dispersion given in Łokas & Mamon (2001) and distributed using a Maxwell–Boltzmann function (Hernquist 1993).[9]

In addition to mock haloes whose density profile is based upon the findings in cosmological simulations (at least down to those scales probed here), we also chose to generate test haloes that follow a Plummer profile (Plummer 1911),

$$\rho(r) = \frac{3M}{4\pi r_{\rm s}^3} \left(1 + \frac{r^2}{r_{\rm s}^2}\right)^{-5/2}, \tag{7}$$

where M is the total mass and $r_{\rm s}$ is the scale radius. The mock haloes were then produced again using a pre-defined number of particles to reproduce the profile, but this time the velocities were obtained using an isotropic, spherically symmetric distribution function (Binney & Tremaine 1987). The two major differences between the Plummer and the NFW density profile are that for the former profile the mass converges and it contains a well-defined constant-density core. This constant density may pose problems for halo finders as most of them rely on identifying peaks in the density field as (potential) sites for DM haloes. We stress that the Plummer spheres are intended as academic problems with no observed counterpart in cosmological simulations and hence only to be taken lightly and for information purposes; they may be viewed as a stability test for halo finders and as a trial how sensitive halo characteristics are against precise measurements of the centre. We will see that some properties can

still be stably recovered even if an incorrect determination of the Plummer halo centre is made.

As we also plan to study the accurate recovery of substructure, we generated setups where one (or multiple) subhaloes are embedded within the density profile of a larger host halo. To this end, we generate, for instance, two haloes in isolation: one of them (the more massive one) will then serve as the host, whereas the lighter one will be placed inside at a known distance from the centre of its host and with a certain (bulk) velocity. The concentrations (i.e. the ratio between the virial and the scale radii) have been chosen in order to meet the findings of cosmological simulations (e.g. Bullock et al. 2001). All our mock haloes are set up with fully sampled 6D initial phase-space distributions and every halo (irrespective of it becoming a host or a subhalo) has been evolved in isolation for several Gyr in order to guarantee equilibrium. The mass of all particles in both the host halo and the subhalo is identical and all haloes have been sampled with particles out to $2 \times R_{100}$, where R_{100} marks the point where the density drops below $100 \times \rho_{\rm crit}$. For more details of the procedure and the generation of the NFW haloes, we would like to refer the reader to Muldrew et al. (2011) and Read et al. (2006), respectively.

The characteristics of the haloes are summarized in Table 1. We are aware of the fact that even though the radius at which the enclosed overdensity reaches some defined level is well defined for our subhaloes when they were generated in isolation, such a definition becomes obsolete once they are placed inside a host. However, we nevertheless need to acknowledge that such a definition may serve as a fair basis for the comparisons of the recovery of subhalo properties amongst different halo finders.

Further, placing an unmodified subhalo at an arbitrary radial distance within a parent halo is also in part an academic exercise. It neglects that 'real' subhaloes will always be tidally truncated. In that regard, it is not realistic to have an extended/untruncated subhalo at small distances to the host's centre. Some halo finders (e.g. SUBFIND) rely on the tidal truncation in order to be able to avoid a very large radially dependent bias in the amount of mass that can be recovered for a subhalo.

For each of the two types of density profiles, we generated the following setups:

(i) isolated host halo;
(ii) isolated host halo + subhalo at $0.5R_{100}^{\rm host}$;
(iii) isolated host halo + subhalo at $0.5R_{100}^{\rm host}$ + subsubhalo at $(0.5R_{100}^{\rm host} + 0.5R_{100}^{\rm subhalo})$; and
(iv) isolated host halo + five subhaloes at various distances.

The (sub-)subhaloes were placed along the *x*-axis and given radially infalling bulk velocities of 1000 km s^{-1} for the subhalo and

---

[9] We are aware of that the velocity distribution is not derived from the full distribution function and that the Maxwell–Boltzmann distribution is only an approximation (cf. Kazantzidis, Magorrian & Moore 2004; Zemp et al. 2008). Despite this, it will have no effect on the ability of halo finders to recover the haloes as has been shown in Muldrew et al. (2011) where also more details about the generation of the mock haloes can be found.

Table 2. The properties of the subhaloes for the NFW resolution study presented in Section 4.1.4. Radii are given in h^{-1} kpc and velocities in km s^{-1}.

N_{100}	N_{tot}	R_{100}	v_{max}	R_{vmax}
10	13	20.41	18.24	3.68
20	27	25.72	22.99	4.62
30	41	29.44	26.31	5.30
40	55	32.40	28.96	5.85
50	68	34.90	31.20	6.30
100	137	43.98	39.31	7.93
500	687	75.20	67.21	13.55
1000	1375	94.74	84.68	17.08

1200 km s^{-1} for the sub-subhalo. These velocities are typical for what you would expect in a DM host halo and were set to round numbers to make the analysis easier; their values were motivated by $\sqrt{2GM_{host}(<D)/D}$, where D is the distance of the subhalo from the host's centre.

The first three setups were used to study the overall recovery of (sub)halo properties presented in Section 4.1.1. The fourth test has been used to study the radial dependence of subhalo properties introduced in Section 4.1.2.

Besides the recovery of (sub)halo properties, we also aim at answering the question 'how many particles are required to find a subhalo?' To this end, we systematically lowered the number of particles (and hence also the subhalo mass as our particle mass remains constant) used to sample the subhalo listed above as test case # 2. The properties of these mock subhaloes are summarized in Table 2 and the results will be shown in Section 4.1.4.

Besides these well-controlled tests, we also performed a so-called 'Blind Test' where the precise setup of the data to be analysed by each halo finder was unknown to the participants. We introduce this particular experiment alongside its results in a stand-alone Section 4.1.5. Only a small subset of the halo finders took part in this trial.

We close this section with a cautionary remark that not all halo finders are *ab initio* capable of identifying subhaloes and hence some of the test cases outlined here were not performed by all the finders. Therefore, some of the codes only contribute data points for the host halo in Section 4.

3.2 Cosmological simulation

The cosmological simulation used for the halo-finder code comparison project is the so-called MareNostrum Universe which was performed with the entropy-conserving GADGET-2 code (Springel 2005). It followed the non-linear evolution of structures in gas and DM from $z = 40$ to the present epoch ($z = 0$) within a comoving cube of side 500 h^{-1} Mpc. It assumed the spatially flat concordance cosmological model with the following parameters: the total matter density $\Omega_m = 0.3$, the baryon density $\Omega_b = 0.045$, the cosmological constant $\Omega_\Lambda = 0.7$, the Hubble parameter $h = 0.7$, the slope of the initial power spectrum $n = 1$ and the normalization $\sigma_8 = 0.9$. Both components, the gas and the DM, were resolved by 1024^3 particles, which resulted in a mass of $m_{DM} = 8.3 \times 10^9 \, h^{-1} \, M_\odot$ for the DM particles and $m_{gas} = 1.5 \times 10^9 \, h^{-1} \, M_\odot$ for the gas particles. For more details, we refer the reader to Gottlöber & Yepes (2007) that describes the simulation and presents results drawn from it.

For the comparison presented here, we discarded the gas particles as not all halo finders yet incorporate a proper treatment of gas physics in their codes. The focus here lies with the DM struc-

tures. However, to avoid that too many particles will be considered 'unbound' (for those halo finders that perform an unbinding procedure), the masses of the DM particles have been corrected for this, that is, $m_{DM}^{corrected} = m_{DM}/(1 - f_b)$, where $f_b = \Omega_b/\Omega_m$ is the cosmic baryon fraction of our model universe.

In order to allow non-parallel halo finders to participate in this test, we degraded the resolution from the original 1024^3 particles down to 512^3 as well as to 256^3 particles. The properties to be compared will, however, be drawn from the highest resolved data set for each individual halo finder, making the appropriate mass/number cuts when producing the respective plots.

3.3 Code participation

Not all codes have participated in all the tests just introduced and outlined. Hence, in order to facilitate an easier comparison of the results and their relation to the particular code, we provide in Table 3 an overview of the tests and the halo finders participating in them. In that regard, we also list for the cosmological simulation the respective resolution of the data set analysed by each code. The last two columns simply indicate whether the code performs an unbinding procedure and provided subhalo properties, respectively.

4 THE COMPARISON

This section forms the major part of this paper as it compares the halo catalogues derived with various halo finders when applied to the suite of test scenarios introduced in the previous section. We first address the issue of the controlled experiments brought forward in Section 4.1 followed by the analysis of the cosmological simulation introduced in Section 4.2. As already mentioned before, we are solely addressing DM haloes, leaving the inclusion of baryonic matter (especially gas) for a later study.

4.1 Mock haloes

Before presenting the results of the cross-comparison, we need to explain further the actual procedures applied. Each data set was given to the respective code representative asking them to return the centre of each object found as well as a list of the (possible) particles belonging to each (sub)halo. A single code using only that particular list was then used to derive the bulk velocity V_{bulk}, the (fiducial) mass M_{200} and the peak of the rotation curve, v_{max}, in order to eliminate differences in the determination of said values from code to code, or, in other words, we did not aim at comparing how different codes calculate, for instance, v_{max} or M_{200} and so eliminated that issue. This simple analysis routine is also available from the project website. We were aiming at answering the more fundamental question 'which particles may or may not belong to a halo?' according to each code. However, not all representatives returned particle lists as requested (due to a different method or technical difficulties) but rather directly provided the values in question; those codes are BDM, FOF and 6DFOF. Further, FOF did not provide values for v_{max}.

When comparing results, we primarily focused on fractional differences to the theoretical values by calculating $\Delta x/x_{Model} = (x_{code} - x_{Model})/x_{Model}$, where x is the halo property in question.

#### 4.1.1 Recovery of host and subhalo properties

For all the subsequent analyses and the plots presented in this subsection, we used the setups (i) through (iii) specified in Section 3.1. In that regard, we have three host haloes (one for the

Table 3. Brief summary of the codes participating in the comparison project. The first six columns provide a synopsis of the respective tests the code participated in (columns 2–7). The last two columns simply list whether the code performs an unbinding procedure and provided subhalo properties, respectively.

| Code | Participation in the test | | | | | | Unbinding | Subhaloes |
	Recovery	Radial dependence	Dynamical infall	Resolution	Blind	Cosmology		
AHF	Yes	Yes	Yes	Yes	Yes	1024^3	Yes	Yes
ASOHF	Yes	Yes	Yes	Yes	Yes	256^3	Yes	Yes
BDM	Yes	Yes	Yes	Yes	Yes	512^3	Yes	Yes
PSO	Only host	No	No	No	Only host	1024^3	No	No
LANL	Only host	No	No	No	No	1024^3	No	No
SUBFIND	Yes	Yes	Yes	Yes	Yes	1024^3	Yes	Yes
FOF	Yes	Yes	Yes	Yes	No	1024^3, no v_{max}	No	Limited
PFOF	Only host	No	No	No	No	512^3	No	No
NTROPY-FOFSV	Only host	No	No	No	No	1024^3, no v_{max}	No	No
VOBOZ	Yes	Yes	No	Yes	Yes	512^3	Yes	Yes
ORIGAMI	No	No	No	No	No	512^3	Yes	No
SKID	Yes	Yes	Yes	Yes	Yes	1024^3	Yes	Yes
ADAPTAHOP	Yes	Yes	Yes	Yes	Yes	512^3	No	Yes
HOT	Yes	Yes	Yes	Yes	Yes	No	No	Yes
HSF	Yes	Yes	Yes	Yes	Yes	1024^3	Yes	Yes
6DFOF	Yes	Yes	Yes	Yes	Yes	1024^3	No	Yes
ROCKSTAR	Yes	Yes	Yes	Yes	No	1024^3	Yes	Yes

host alone, one from the host+subhalo setup and one from the host+subhalo+subsubhalo configuration); we further have two sub-haloes at our disposal (one from the host+subhalo and one from the host+subhalo+subsubhalo tests) as well as one subsubhalo. In all the figures presented below, the origin of the halo is indicated by the size of the symbol: the largest symbol refers to the host+subhalo+subsubhalo set with the symbol size decreasing in the order of the host+subhalo towards the host test alone. We further always show the results for the NFW mock haloes in the left-hand panel and for the Plummer spheres in the right-hand panel. As much as possible, the halo finders have been organized in terms of their methodology: SO finders first followed by FOF-based finders with 6D phase-space finders last.

Centre determination. We start with inspecting the recovery of the position of the haloes as practically all subsequent analyses as well as the properties of haloes depend on the right centre determination. The results can be viewed in Fig. 2 where the y-axis
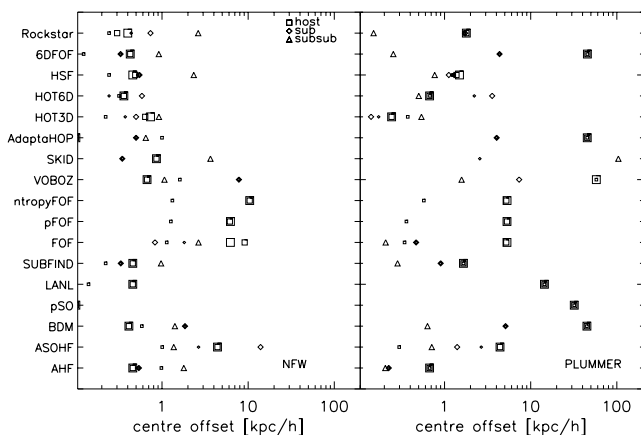
Figure 2. The offset of the actual and recovered centres for the NFW (left-hand panel) and Plummer (right-hand panel) density mock haloes. The symbols refer to either the host halo, subhalo or subsubhalo as indicated, while the symbol size indicates the test sequence as detailed in the text (i.e. larger symbols for haloes containing more subhaloes).

represents the halo finder and the x-axis measures the offset between the actual position and the recovered centre in h^{-1} kpc.

We can clearly see differences for all sorts of comparisons: host haloes versus (sub-)subhaloes, NFW versus Plummer model, and – of course – amongst halo finders. While for the NFW density profile the deviations between the analytical and recovered centres are for the majority of haloes and codes below $\approx 5\,h^{-1}$ kpc, there are nevertheless some outliers. For the large halo, the 100th particle is $3\,h^{-1}$ kpc from the nominal centre. These outliers are primarily for the FOF-based halo finders which are using a centre of mass rather than a density peak as the centre. However, for a perfectly spherically symmetric setup as the one used here, the differences between the centre of mass and density peak should be small. Some of the finders (PSO, LANL, PFOF, NTROPY-FOFSV) were not designed to find substructure and so do not return the locations for these. Interestingly, HOT6D cannot detect the NFW sub-subhalo. The situation is a bit different for the Plummer model that consists of a flat density profile inwards from the scale radius of $190\,h^{-1}$ kpc. While the centre offset for the FOF finders remains the same, we now also observe a shift towards larger offset values for the majority of the other codes; some codes were even unable to locate the host halo at all (e.g. SKID), while other finders marginally improved their (sub)halo centre determination (AHF, ASOHF, HOT3D). Remember that for 6DFOF all positions and velocities were solely determined from the linked particles, which explains the slightly offset centres in cases where only a few particles were linked (as in the case of the Plummer sphere which had an artificial low phase-space density by construction) as well as the somewhat different bulk velocities (when compared to the other halo finders below).

Halo bulk velocity. A natural follow-up to the halo centre is to ask for the credibility of the bulk velocity of the halo. Errors in this value would indicate the contamination from particles not belonging to the halo in question to be studied in greater detail in Section 4.1.4 below. In our test data, the host is always at rest, whereas the subhalo (sub-subhalo) flies towards the centre with 1000 (1200) km s^{-1} along the negative x-direction. The fractional difference between the model velocity and the bulk velocity as measured for each halo finder is presented in Fig. 3. Note that we have normalized the host's velocities to the rotational velocity at R_{100}, that is, ≈ 1000 km s^{-1},
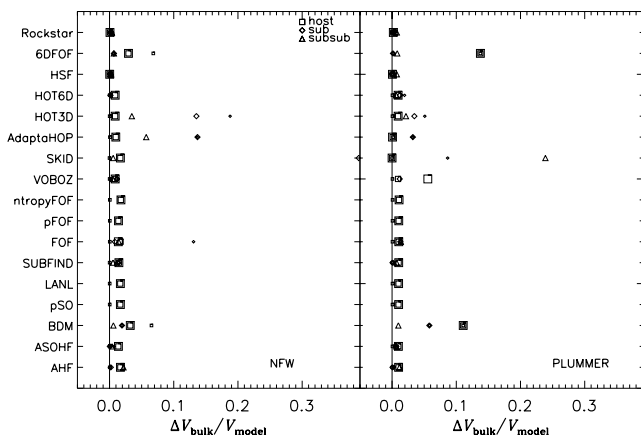
Figure 3. Recovery of halo bulk velocities in comparison to the analytical input values for the NFW (left-hand panel) and Plummer (right-hand panel) density mock haloes. Note that the host halo has been set up to be at rest with $v_{bulk} = 0$. The symbols have the same meaning as in Fig. 2.
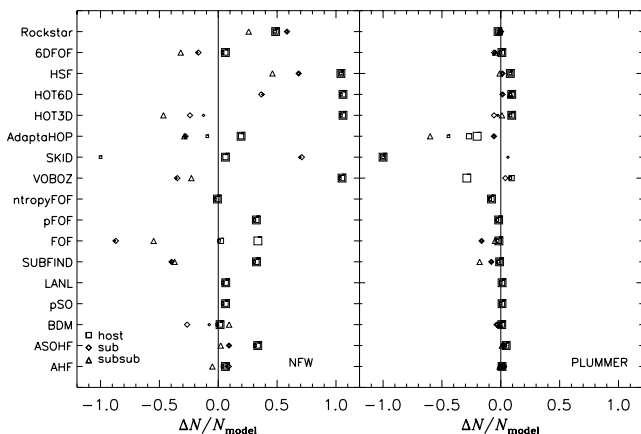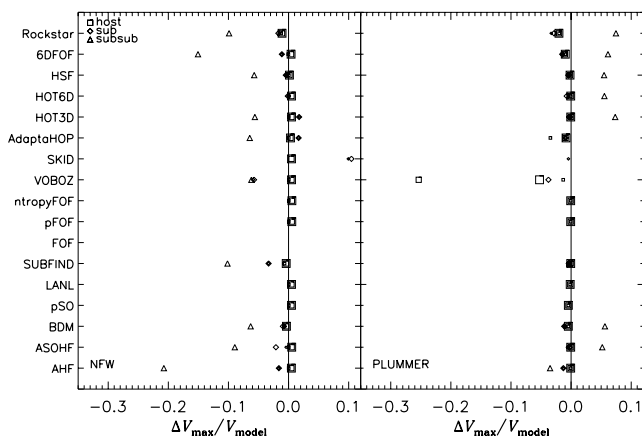

Figure 4. Total number of particles recovered for the (sub)halo for the NFW (left-hand panel) and Plummer (right-hand panel) density mock haloes with respect to the number of particles within M_{200}. The symbols have the same meaning as in Fig. 2.

for the two density profiles. Here we find that for practically all halo finders, the error in the bulk velocity is smaller than 3 per cent; only some outliers exist. Note that we used all particles in the determination of the bulk velocities as returned/recovered by the respective halo finder. SKID displays very significant contamination in the recovered subhaloes with a 40 per cent error in the recovered bulk velocity but is also one of the codes whose returned particle lists are intended to undergo significant post-processing. ADAPTAHOP and HOT3D have smaller but still significant levels of contamination within the returned substructures. The marginal offset in the bulk velocities of the Plummer host haloes for 6DFOF and BDM is directly related to the respective centre offsets seen in Fig. 2: those two codes base their bulk velocities on particles in the central regions.

Number of particles. In Fig. 4, we are comparing the number of particles recovered by each halo finder to the number of particles within M_{200} listed in Table 1.[10] We are aware that there is no such well-defined radius for (sub-)subhaloes, but it nevertheless provides a well-defined base to compare against.

---

[10] Note that in all subsequent plots, we are using N_{200} when referring to N_{model}.
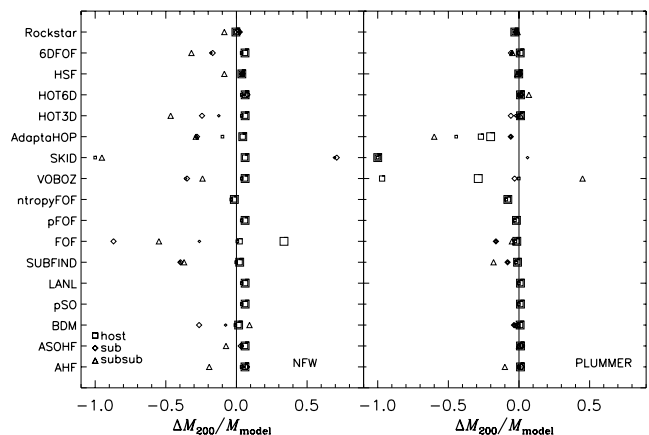
Figure 5. M_{200} mass (as determined from the supplied particle lists) measured according to the mean enclosed density being $200 \times \rho_{crit}$ criterion for the NFW (left-hand panel) and Plummer (right-hand panel) density mock haloes extracted from each finder's list of gravitationally bound particles. The symbols have the same meaning as in Fig. 2.

We observe that while the errors are at times substantial for the NFW model the Plummer results appear to be more robust this time. However, this is readily explained by the form of the applied density profile: the variations in mass and hence in the number of particles are more pronounced for the NFW profile than for the Plummer model when changing the (definition of the) edge of a halo or, in other words, the total mass of a Plummer model is well defined, whereas the mass of an NFW halo diverges. Therefore, (minor) changes and subtleties in the definition of the other edge of a (sub)halo will lead to deviations from the analytically expected value – at least for the NFW model. To this extent we also need to clarify that each halo finder had been asked to return that set of particles that was believed to be part of a gravitationally bound structure; participants were not asked to return the list of particles that make up M_{200}. Post-processing of the supplied particle lists to apply this criterion results in errors for the NFW profiles that are well below 10 per cent – at least for the host haloes (cf. Fig. 5 below). However, a straight comparison of the number of recovered particles amongst the codes reveals a huge scatter. This is due to the fact that the individual codes are tuned to different criteria to define the edge of the halo. Clearly, some codes (HSF, HOT, VOBOZ) have been tuned to extract an effectively smaller overdensity for this test than, say, 6DFOF, LANL, PSO or AHF. This is a well-known issue and all code developers are well aware of it. Perhaps more concerning is the wide scatter in the relative mass of the largest subhalo. Here M_{200} is ill-determined but the ratio of the substructure mass to the host halo mass displays a wide scatter. This ratio is of astrophysical importance for several issues.

The difference in a host halo seen for FOF and PFOF is – in general – due to the choice of a linking length not corresponding to $200 \times \rho_{crit}$. However, with an appropriate linking length the FOF algorithm detects the halo at the desired overdensity correctly as can be seen for the host-only and host+subhalo data for which there is agreement with the analytical expectation as opposed to the host+subhalo+subsubhalo where the standard linking length has been applied and hence the number of particles (and mass) is overestimated. As a (down)tuned linking length has also been utilized for the detection of the (positions of the) subhaloes, the higher overdensity encompassed naturally led to a smaller number of particles (and masses) than assumed in the model.

Again, we stress that Fig. 4 does not necessarily reflect the number of particles actually used to calculate halo properties; it is the raw number of (bound) particles assigned to the centre of the respective (sub)halo and used for further post-processing with most of the codes. However, the comparison also indicates that neither the number of particles nor M as defined by some overdensity criterion (see below) is a stable quantity for a fair comparison; this is why we argue in favour of the peak of the rotation curve for cross-comparison as already highlighted in the Introduction.

Mass. Using the particle lists provided by each halo finder, we extract each object and calculate the density profile. From this we determine the point where it drops below $200 \times \rho_{crit}$. This point can then be used as a radial distance within which to define M_{200} which is then compared against the theoretical expectation (cf. Table 1) in Fig. 5. Again, we acknowledge that this is not the correct definition for the (sub-)subhalo mass, but can regardlessly be used to compare halo finders amongst themselves.

As already outlined in the previous paragraph, the differences to the analytical values (and between the codes) are substantially alleviated, now that differences in the definition for the edge of each halo have been removed. The apparent underestimation of the (sub-)subhalo masses has also to be taken and digested carefully as the M_{200} values are based upon objects in isolation when these are embedded in a large host halo. However, recall that the values for BDM, FOF and 6DFOF are based upon their respective criteria as these codes did not return particle lists but directly M_{200}.

Amongst those codes that did recover subhaloes and underwent the same processing scheme, there remains a surprisingly wide variation in the recovered subhalo mass M_{200}. Almost all the codes studied here post-process their subhalo catalogues heavily to alleviate this problem. We would, however, stress that the precise definition for a subhalo content can, as demonstrated, lead to a range of recovered subhalo masses, a point users of subhalo catalogues should be well aware of. We will return to the issue of the missing subhalo mass in Section 4.1.3 below, which provides some explanation for the variation.

Maximum of the rotation curve. As outlined in Section 1.3, M_{200} does not provide a fair measure for the (sub-)subhalo mass and hence we consider the maximum circular velocity v_{max} as a proxy for mass. The fractional difference between the theoretically derived v_{max} and the value based upon the particles returned by each halo finder is plotted in Fig. 6. While we now find a considerably

improved agreement with the analytical calculation, the sub-subhalo has still not been recovered correctly in most of the cases. This result is entirely in line with the results of fig. 7 of Muldrew et al. (2011) where the error in measuring v_{max} for a range of particle numbers was calculated: we should not be surprised by a 10 per cent underestimate for our subsubhalo as this is well within the expected limits.

4.1.2 Radial dependence of subhalo properties

The following test aims at studying how the recovered properties of a subhalo change as a function of the distance from the centre of the subhalo to the centre of its host. We always placed the same subhalo (sampled with 10 000 particles) at various distances and applied each halo finder to this test scenario, without changing the respective code parameters in between the analyses. We then focused our attention on the number of gravitationally bound particles in Fig. 7, the recovered M_{200} masses in Fig. 8 and the maximum of the rotation curve in Fig. 9.

We reiterate that this particular test (as well as the following two) is only suited to halo finders that are able to identify the substructure embedded within the density profile of a larger encompassing object. Therefore, some of the codes will not appear in this and the following tests in Sections 4.1.3 and 4.1.4. However, we also need to acknowledge that some of the code developers were keen
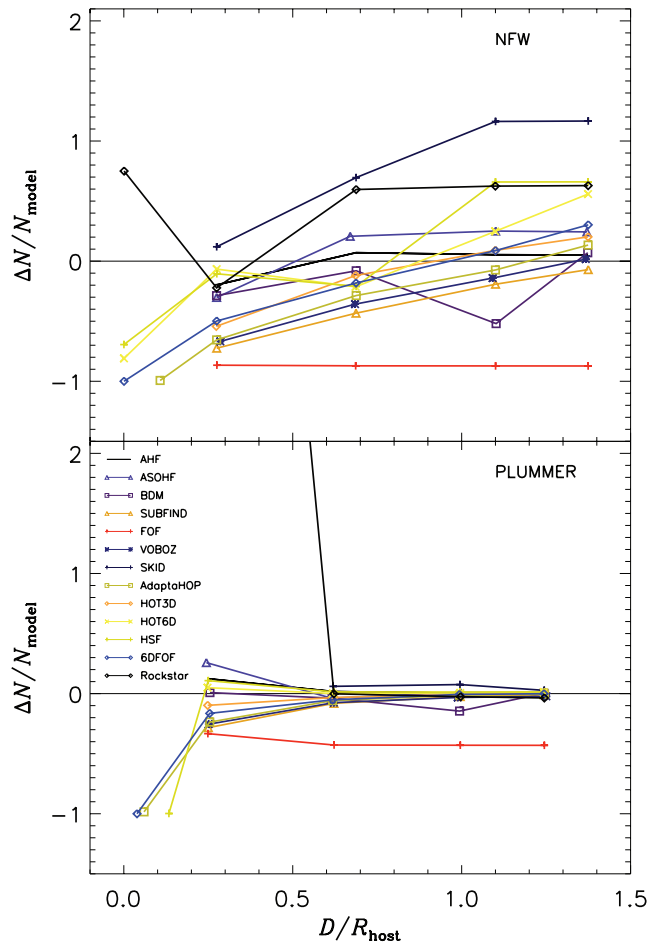

Figure 6. Recovery of numerical v_{max} values in comparison to the analytical input values for the NFW (left-hand panel) and Plummer (right-hand panel) density mock haloes. The symbols have the same meaning as in Fig. 2.

Figure 7. Number of particles belonging to the subhalo for the NFW (upper panel) and Plummer (lower panel) density mock haloes as a function of the subhalo distance from the host.
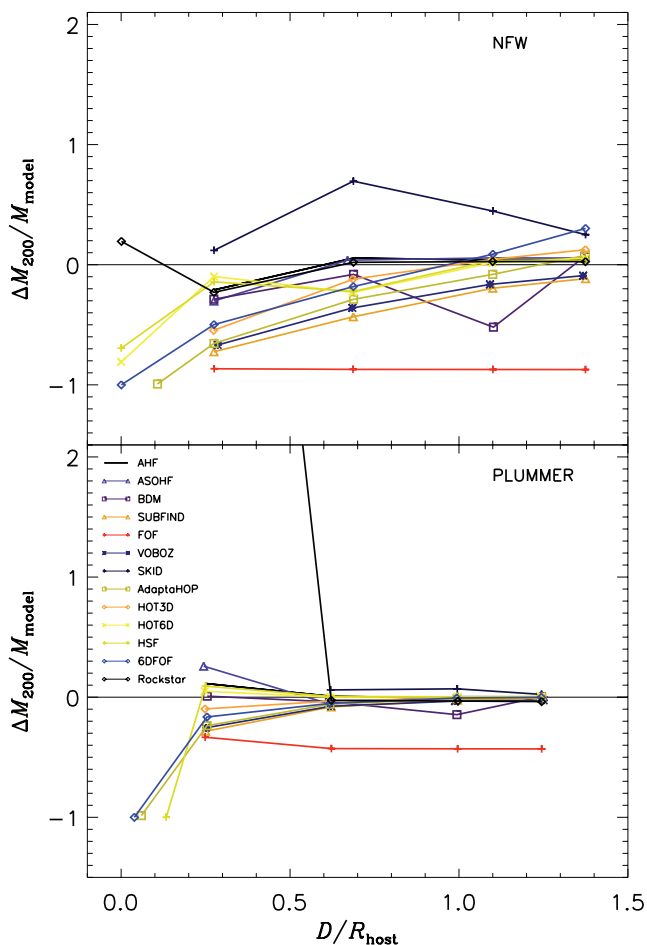
Figure 8. Hypothetical M_{200} value comparison to the NFW (upper panel) and Plummer (lower panel) subhalo as a function of the distance from the host. M_{200} was calculated again considering the recovered particles N (as presented in Fig. 7) in isolation.
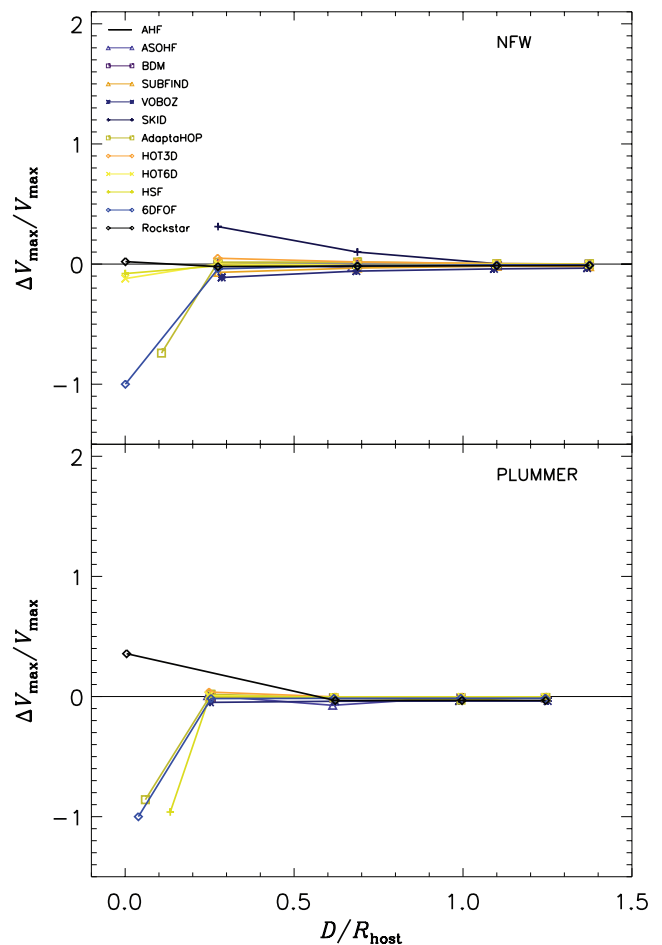
Figure 9. Recovery of numerical v_{max} values in comparison to the analytical input values for the NFW (upper panel) and Plummer (lower panel) density mock haloes as a function of the subhalo distance from the host.

to participate in this venture and manually tuned their halo finders to (at least) provide a centre and possibly mass estimate for the subhalo under investigation (e.g. FOF by Gottlöber & Turachninov systematically lowered their linking length until an object had been found using the spin parameter as a measure for credibility (cf. Section 2.7); however, as FOF in its basic implementation does not perform any unbinding, they did not dispense particle lists and/or internal properties). Therefore, the results for FOF are to be taken lightly and with care.

Number of particles. Aside from the location of the substructure, which we are not investigating in more detail in this particular subsection, the number of particles recovered by each halo finder is the first quantity to explore as a function of the subhalo distance. The results can be viewed in Fig. 7 with the NFW mock halo in the upper panel and the Plummer sphere in the lower. Recall that there are five subhaloes placed at various distances from the centre of the host with the closest one actually overlapping with the host centre.

As expected from the above results of the previous section (which equate to the middle position of these five haloes), various halo finders recover a range of the number of particles within the halo. Only the phase-space-based finders are capable of disentangling the subhalo when it is directly at the centre. Even then their particle recovery indicates that either there are too few particles associated with the subhalo or they found the host. We further observe that, at

least for the NFW haloes, the number of recovered particles drops the closer we get to the centre. This is naturally explained by the fact that the density contrast of the subhalo becomes smaller and the point where the host halo's density takes over is closer to the centre of the subhalo. This is another reflection of the fact that the number of particles (or anything based upon a measure of the 'halo edge') is not a good proxy for the actual subhalo. The situation is obviously different for the Plummer sphere with no pronounced density rise towards the centre; therefore, the subhalo appears to be well recovered in this case. For the low number of particles recovered by SUBFIND, we refer the reader to an improved discussion and investigation, respectively, in Muldrew et al. (2011).

In any case, these are still simply the particle lists; we continue to check the (hypothetical) M_{200} values as well as the recovery of the maximum of the rotation curve. When defining a (hypothetical) M_{200} value, considering the subhalo in isolation, we find basically the same trends as for the number of particles. This can be verified in Fig. 8 where we observe the same phenomena as in Fig. 7. However, SKID is the exception with the M_{200} values closer to the actual model mass across all distances than to the number of particles, as expected and as they themselves would obtain during their own post-processing steps.

We note that the discrepancy between the (fiducial) mass and the real mass of the subhalo placed at different radial distances from the centre is more serious in this idealized setup than it would be

in a realistic situation, where the substructures would experience tidal truncation in moving towards the inner regions of the halo (see the discussion in Section 3.1 as well as the study of the dynamical subhalo infall in Section 4.1.3 below); when considering the mass within the tidal truncation radius, the discrepancy between the 'real' and recovered mass would reduce.

Maximum of the rotation curve. The most credible measure of the subhalo mass, however, appears to be the maximum of the rotation curve: it hardly changes its value, irrespective of the position inside the host halo as can be seen in Fig. 9. All halo finders perform equally well in recovering the v_{max} value from the list of particles used in Fig. 7. This then indicates that the only difference between the halo finders as seen as a substantial spread in (the upper panel of) Fig. 7 stems from the outer and less-well-contrasted regions of the subhalo.

We have seen in Section 4.1.1 that the maximum of the rotation curve, v_{max}, serves as an adequate proxy for mass and hence we test its sensitivity to the radial position in Fig. 9. We find that this quantity is, as expected, hardly affected by the actual position of the subhalo within the host. Its value is determined by the more central regions of the subhalo and hence does not change if the object is truncated in the outskirts due to the embedding within the host's background density field. Only when the two centres of the subhalo and the host halo overlap do we encounter problems again; however, HOT6D and HSF even master this situation fairly well (at least for the more realistic NFW test scenario).

4.1.3 Dynamical infall of a subhalo

The test described and analysed in this subsection is a dynamic extension of the previously studied radial distance test: we throw a subhalo (initially sampled with 10 000 particles inside M_{100}) into a host halo two orders of magnitude more massive. It was initially placed at a distance of $D = 3 \times R_{100}^{host}$ with a radially inward velocity of $v = \sqrt{2GM(<D)/D} = 686\,km\,s^{-1}$ and then left to free fall. During the temporal integration of this system with GADGET-2, the cosmological expansion was turned off so the haloes were only affected by gravity. The orbit of the subhalo takes it right through the host halo centre, exiting on the other side. Due to the tidal forces, the subhalo will lose mass and we aim at quantifying how different halo finders recover both the number of (bound) particles as well as the evolution of the peak rotational velocity.

Evolution in the number of particles. In Fig. 10, we start again with the number of recovered particles, this time as a function of time measured in Gyr since the infalling object passed $2 \times R_{200}^{host}$. Note that the fractional difference $\Delta N/N_{model}$ is measured with respect to the number of particles, N_{model}, prior to infall and that the analysis has only been performed over a certain number of output snapshots and not every integration step. At the starting point, we observe again the same scatter in the number of particles as already found in Fig. 7.[11] Until the passage through the very centre of the host halo after approximately 1.8 Gyr, we also find the expected drop in the number of particles due to the stripping of the subhalo; however, as noted in Fig. 7, part of this drop can also be attributed to the subhalo moving deeper into the dense region of the host. This drop in the particle number has a marginally different shape depending on the halo finder. However, this time, actually, all halo finders (expect
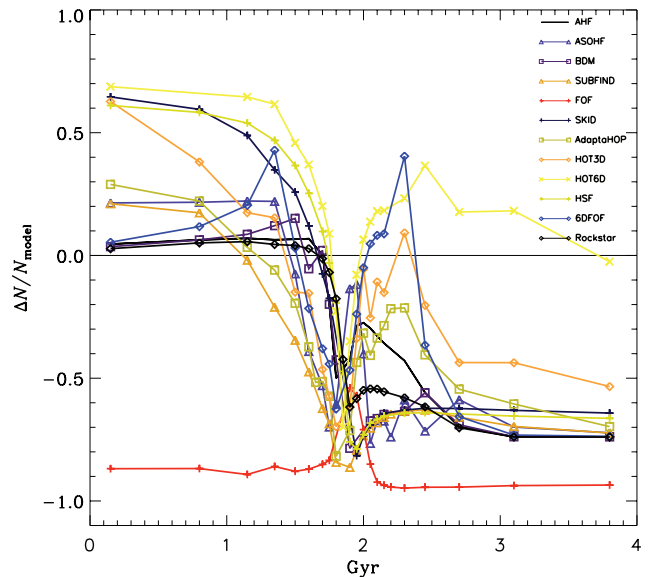
---

[11] However, when comparing Fig. 7 with Fig. 10 one needs to bear in mind that the radial dependence of subhalo properties only extends out to $\approx 1.37 \times R_{200}^{host}$, whereas the first data point in Fig. 10 is for $2 \times R_{200}^{host}$.

Figure 10. Temporal evolution of the number of particles belonging to the subhalo for the dynamical infall study.

most of the phase-space finders, cf. Fig. 12 shown below) do lose the subhalo when it overlaps with the host halo – or at least are unable to determine its properties at that time (e.g. 6DFOF actually found the objects but could not assign the correct particles to it as the search radius for 'subhalo membership' was practically zero). After the passage through the centre, all halo finders identify the object again with more particles yet obviously not reaching the original level anymore.

However, we also like to mention that after the core transition of the subhalo we expect to find a more or less constant set of particles that remain bound to the subhalo: as the radial distance increases again there is no reason for the subhalo to lose additional mass. It seems clear that the majority of structure finders agree on this plateau value, but there are also some that return an unphysical result in this regime (e.g. both HOT codes as well as 6DFOF in the early phases).

Note again that none of the FOF-based halo finders is *ab initio* designed to locate substructure, but the FOF results have been included as this code was manually tuned to locate subhaloes (cf. Section 4.1.2).

Evolution of the maximum of the rotation curve. As we have already seen before a number of times, the number of particles has to be used with care as the actual halo properties will be based upon them, but the list has undeniably to be pruned and/or post-processed. We therefore present in Fig. 11 again the evolution of the maximum of the rotation curve which focuses on the more central regions of the subhalo and its particles. Here, we can undoubtedly see that all halo finders perform equally well (again): they all start with a value equal to the analytical input value and have dropped by the same amount, once the subhalo has left the very central regions again. However, the majority of the codes (except SUBFIND, HSF and SKID) found a sharp rise in v_{max} right after the central passage.

To gain better insight into this region, we show in Fig. 12 a zoom into the time-frame immediately surrounding the central passage, this time though using the distance (as measured by the respective halo finder) from the host centre as the x-axis. We attribute part of this rise to an inclusion of host particles in the subhalo's particle list to be studied in greater detail below in Section 4.1.4; we can see
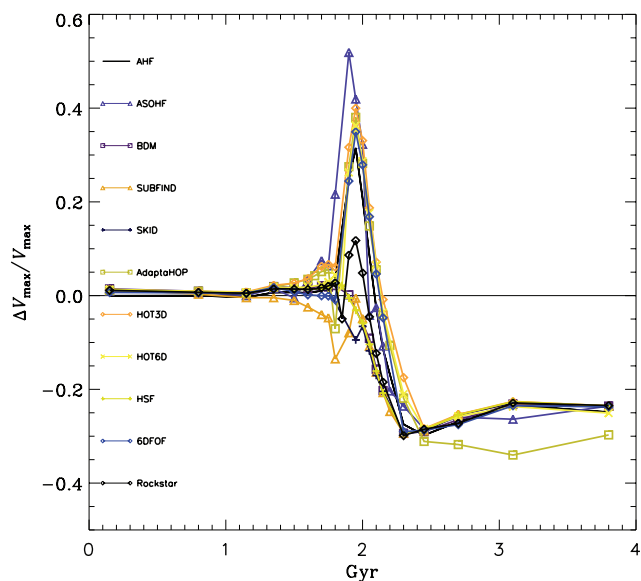
Figure 11. Temporal evolution of the maximum of the rotation curve for the dynamical infall study.
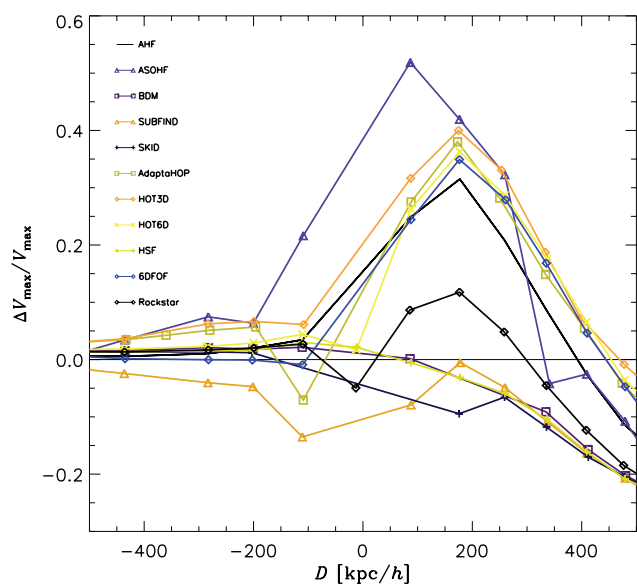

Figure 12. The maximum of the rotation curve for the dynamical infall study as a function of the distance (as measured by the halo finder) from the centre of the host – zooming into the region about the centre.

that codes having problems with such contamination appear to show this rise too – even though not all of the codes showing this rise are amongst the list of finders showing contamination. However, this rise is also (or maybe even more) indicative of problems with the unbinding procedure: particles which have just left the subhalo (and are then part of the host) may still be considered bound, depending on the particulars of the halo finder. For instance, AHF assumes a spherically symmetric object during the unbinding process which is obviously not correct for an object heavily elongated by the strong tides during the central passage. However, one should also bear in mind that a rise in v_{max} also occurs when the subhalo gets (tidally) compressed and hence R_{max} is lowered (cf. Dekel, Devor & Hetzroni 2003) even though this has not been seen in all (controlled)

experiments of this kind (e.g. Hayashi et al. 2003; Klimentowski et al. 2009).

Finally, we point out that the x-axis is based upon the distance to the host centre as measured by each individual halo finder and it is rather obvious that all halo finders have recovered (more or less) the same distance for the subhalo.

4.1.4 Resolution study of a subhalo

While we have seen that there is little variation of the most stable subhalo properties with respect to the distance from the host (i.e. v_{max}), we now investigate the number of particles required to (credibly) identify a subhalo. To this extent we used setup (ii) from the list in Section 3.1 where we placed a single subhalo into a host halo at half the host's M_{100} radius. But this time we gradually lowered its mass and number of particles (keeping the mass of an individual particle constant). Even though it is meaningless to talk about R_{200} radii for subhaloes again, we are nevertheless comparing the number of gravitationally bound particles, as returned by the respective halo finder, with the number of particles inside the subhaloes' R_{200} radius; remember that the subhaloes were generated in isolation and sampled out to two times their M_{100} radius (cf. Section 3.1).

Number of particles. The results of this resolution study can be viewed in Fig. 13 where we plot the fractional difference in the number of particles within R_{200} against the number of particles in the subhalo. In this figure, there are two important things to note and observe: (i) the end-point of each curve (towards lower particle numbers) marks the point where the respective halo finder was no longer able to identify the object; and (ii) a constant line (irrespective of being above, on top or below the 0-line) means that for each particle number the error in the determination is equal. Again, practically all halo finders perform equally well, that is, they recover the input number of particles with a constant error across all values. Only the two HOT algorithms show a strong deviation due to the lack of an unbinding procedure. It is also interesting to compare the (inner) end-point of the curves marking the number of particles
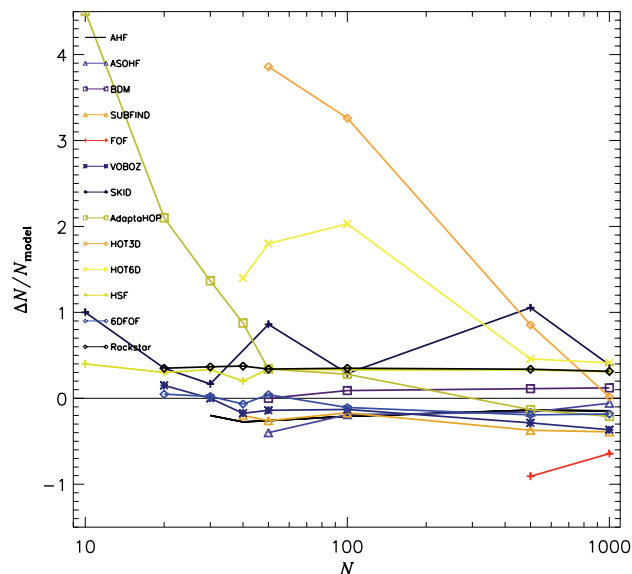

Figure 13. Fractional difference between the number of particles within the recovered R_{200} and the number of particles belonging to the halo as returned by the respective halo finder versus the number of particles inside the subhalo.

for which a certain code stopped finding the subhalo: all of them were still able to identify the object with 50 particles. HSF and SKID actually went all the way down to 10 particles with VOBOZ, 6DFOF and ROCKSTAR stopping at 20 particles, and AHF at 30. We need to stress that codes were asked not to alter their technical parameters while performing this resolution study and hence some may in fact be able to recover objects with a lower number of particles than presented here. For instance, we are aware of that SUBFIND (as well as AHF and ASOHF) is capable of going all the way down to 20 particles, if the technical parameters are adjusted appropriately.

In any case, we also observe that some codes show a rise in $\Delta N/N_{\mathrm{model}}$ towards lower particle numbers (e.g. ADAPTAHOP, HOT); could this be due to the contamination from host halo particles? We will study this phenomenon in the following subsection.

Contamination by host particles. Downsizing a subhalo yet still trying to pinpoint it also raises the question how many of the recovered particles are actually subhalo and how many are host halo particles. We are in the unique situation to know the IDs of both the subhalo and the host halo and hence studied the 'contamination' of the subhalo with host particles as a function of the number of (theoretical) subhalo particles in Fig. 14. We can see that the vast majority of the halo finders did not assign any host particles to the subhalo. However, some halo finders appear to have picked up a fraction of host particles possibly leading to differences in the subhalo properties such as v_{max} investigated next. Note that the high contamination for ADAPTAHOP is due to the lack of an unbinding procedure.

Maximum of the rotation curve. As the number of particles is merely a measure for the cross-performance of halo finders and not (directly) related to credible subhalo properties, we also need to have a look at v_{max} again. The fractional error as a function of the (theoretical) number of subhalo particles is plotted in Fig. 15. We note that aside from those halo finders who showed a contamination by host particles, all codes recover the theoretical maximum of the rotation curve down to the limit of their subhalo's visibility (although possibly the last data point for the lowest number of particles should be discarded in that regard).
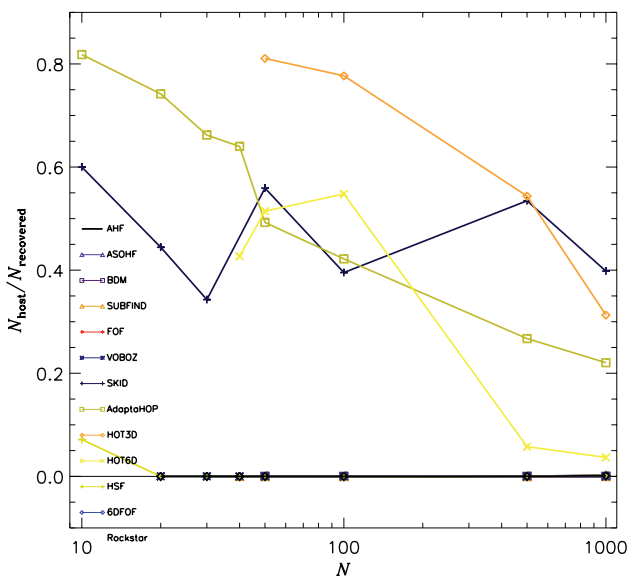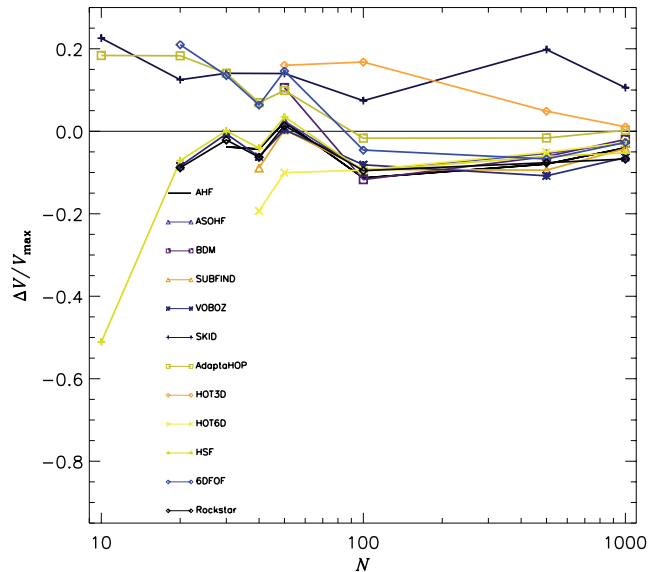
Figure 15. Fractional difference between the theoretical maximum of the rotation curve and the numerically derived maximum versus the theoretical maximum for the subhalo.

4.1.5 The 'Blind Test'

Aside from the mock haloes analysed before, we also designed a particular test where none of the participants had foreknowledge of what it contained; only Stuart Muldrew, who generated all the mock haloes, knew the setup that is summarized in Table 4 where the type 'Host' refers to the host halo and 'Sub' refers to a subhalo. We dubbed this individual test the 'Blind Test'. Note that some of the subhalo's density profiles in this test followed a Hernquist model (Hernquist 1990, marked 'Hern' in the table) instead of the NFW profile. Further, two haloes were deliberately placed at the same location yet with diametrically opposed velocities.

As this test more or less marked the end of the workshop and was primarily considered a fun exercise, we did not include it in the actual data set presented in Section 3.1. Note that not all halo finders participated and that we did not give the players in the game a chance to tune their code parameters to the data set. Nevertheless we decided to simply show visual impressions of those who returned results in Fig. 16. There we merely show the projections of the (fiducial) R_{200} and R_{vmax} radii in the *x–y* plane as the *z*-coordinate of all haloes is identical.

It is interesting to note that the phase-space halo finders were again capable of locating the two overlapping subhaloes even though this is not clearly visible in the projection (as their circles are obviously overlapping). Of the 3D finders, SKID noted that there was something odd at that position, returning one object with double

Figure 14. Fraction of host's particles identified to be part of the subhalo as a function of particles inside the subhalo.

Table 4. Summary of the haloes in the Blind Test. Positions are given in h^{-1} Mpc and velocities in km s^{-1}.

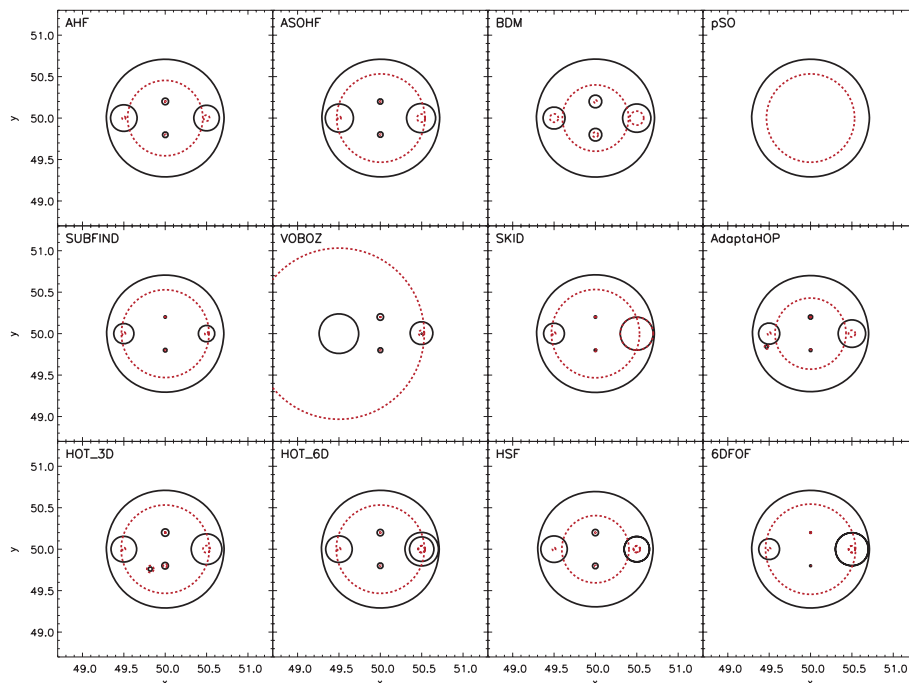| Type	N_{100}	x	y	z	v_x	v_y	v_z	Profile
Host	10^6	50	50	50	0	0	0	NFW
Sub	10^4	50.5	50	50	-10^3	0	0	NFW
Sub	10^4	50.5	50	50	10^3	0	0	NFW
Sub	10^4	49.5	50	50	10^3	0	0	Hern
Sub	10^2	50	49.8	50	10^3	10^3	0	NFW
Sub	10^2	50	50.2	50	0	-10^3	0	Hern

Figure 16. Visual impression of the 'Blind Test' (projection into the *x*–*y* plane). Each halo found is represented by a circle with a radius equal to the fiducial R_{200} value (solid black) and the R_{vmax} value (dashed red).

the mass (and R_{vmax} extending out to the outer radius). All other halo finders only found one of the two subhaloes. Also remember that PSO is not (yet) designed to find subhaloes and hence only the host has been returned. It is further remarkable that none of the halo finders had trouble finding the two small subhaloes while the host had not been found for some of the codes.

Again, we would like to stress that this test should not be taken too seriously. However, we nevertheless remark that analysing a cosmological simulation is also a sort of 'blind' analysis as the answer is not previously known.

4.2 Cosmological simulation

We now turn to the comparison of a real cosmological simulation including a substantial number of objects formed and embedded within the large-scale structure of the Universe.

However, even though the simulation contains a large number of particles (i.e. up to 1024^3 in the highest resolved data set), the given volume of side length $500\ h^{-1}$ Mpc does not allow for a study of subhaloes in detail: for the fiducial 512^3 particle run the largest object in the simulation box merely contains of the order of 10 subhaloes with the number of substructure objects dramatically decreasing when moving to (potentially) lower mass host haloes. We therefore stress that this particular comparison only focuses on field haloes and hence is well suited even for those codes that (presently) cannot cope with subhaloes.

Further, as mentioned already in Section 3.2 we have the data available at various resolutions ranging from 256^3 to 1024^3 particles. We decided to use the highest resolution analysis performed by each finder as has already been summarized in Table 3 in the subsequent comparison plots. The analysis in this particular section primarily revolves around the (statistical) recovery of halo properties. In that regard, we are nevertheless limiting our analysis to properties akin to the ones already studied in Section 4.1, namely the mass M, the position R, the peak of the rotation curve v_{max} and the (bulk)

velocity V_{bulk}. We are going to utilize masses as defined via $200 \times \rho_{crit}$, that is, M_{200}.

We like to reiterate at this point again that for this particular comparison each halo finder returned halo properties as derived from applying the code to the actual data set; we aim at comparing the results of the codes for each and every single one being applied to the data individually. We consider this the most realistic comparison as this directly gauges the differences of the resulting halo catalogues.

We have already seen that all halo finders are capable of recovering the mass of mock haloes, irrespective of whether the density profile is cored or has a cusp (cf. Fig. 5). We therefore do not expect to find surprising differences in the first and most obvious comparison, that is, the (cumulative) mass function presented in Fig. 17. Note that PFOF discarded objects below 100 particles and hence did not return haloes below $\approx 8 \times 10^{12}\ h^{-1}$ M$_\odot$; similarly, PSO discarded objects with fewer than 50 particles, according to the criterion laid out in equation (30) of Lukić et al. (2007), and in each case the (cumulative) mass function starts to flatten at approximately the resolution limit of the simulation analysed by the respective code.

However, ORIGAMI seems to miss some low-mass structures caught by other halo finders. One possible reason is that some smaller density enhancements seen by other finders have not undergone shell-crossing along three axes, and therefore do not meet ORIGAMI's definition of a halo. Another is that ORIGAMI may be missing subhaloes, which it does not attempt to separate from parent haloes.

Further, the LANL halo finder is designed to be an FOF finder and, if needed, SO objects are defined on top of such FOF haloes. Thus, for smaller haloes, completeness is an issue as not every SO halo will have an FOF counterpart. Of course, it is possible to run the code in the limit $b \to 0$ and $N_{min} = 1$, having each particle serving as a potential centre of an SO halo, but the increase in computational cost would make this impractical, as direct SO halo finders which do precisely this in a more effective manner already exist. Nevertheless,
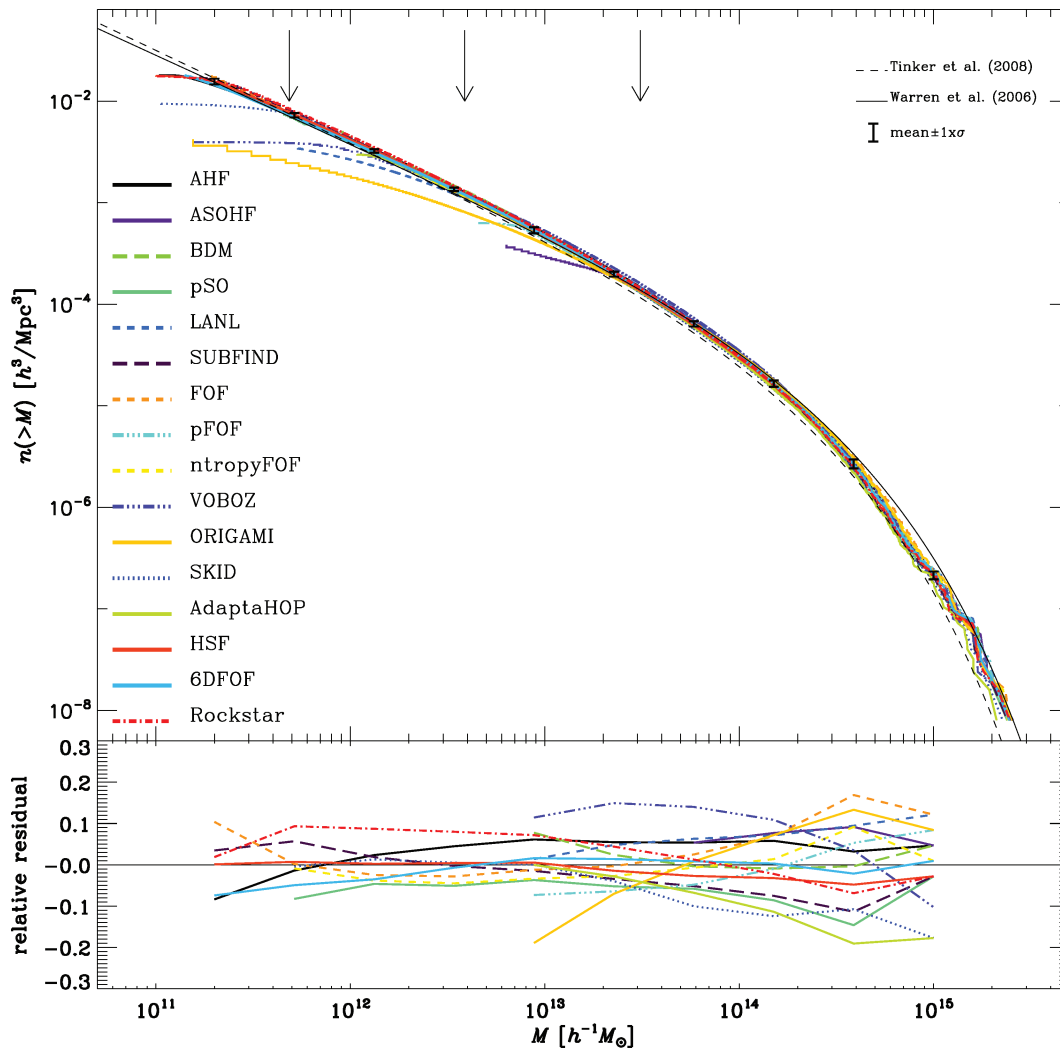
Figure 17. Upper panel: the cumulative mass (M_{200}) function. The arrows indicate the 50 particle limit for the 1024^3 (left-hand panel), 512^3 (middle panel) and 256^3 (right-hand panel) simulation data. The thin black lines crossing the whole plot corresponds to the mass function as determined by Warren et al. (2006, solid line) and Tinker et al. (2008, dashed line). The error bars represent the mean mass function of the codes ($\pm 1\sigma$). Lower panel: the fractional difference between the mean and code halo mass functions. For more details, refer to the text.

we can see that the computationally very fast method of growing SO spheres on top of FOF proxy haloes results in excellent match when compared to direct SO finders for well-sampled haloes ($\sim$500 particles per halo).

In order to better view (possible) differences in the mass functions, we further calculated the 'mean mass function' in 10 logarithmically placed bins across the range 2×10^{11}–$1 \times 10^{15}\, h^{-1}\, M_\odot$ alongside 1σ error bars for the means. Note that all codes only contributed to those bins where their data set is considered complete. We further deliberately stopped the binning at $1 \times 10^{15}\, h^{-1}\, M_\odot$ to not be dominated by small number statistics for the few largest objects. The results can also be viewed in Fig. 17, where we show in the bottom panel the fractional difference between the mean and the code mass functions across the respective mass range, and we additionally added as the thin solid black line to the actual mass function plot in the upper panel of Fig. 17 the numerically determined mass function of Warren et al. (2006) which is based upon a suite of 16 1024^3 simulations of the ΛCDM universe as well as the one of Tinker et al. (2008) derived from a substantial set of cosmological simulations actually including the ones used by Warren

et al. (2006) (cf. their fig. 1). Note that the former is based upon FOF and the latter on SO masses.

As highlighted in Introduction 1.3, the peak value of the rotation curve may be a more suitable quantity to use when it comes to comparing the masses of (DM) haloes. We therefore show in Fig. 18 the cumulative distribution of v_{max}. Apart from the expected flattening at low v_{max} due to resolution, we now note that this is in fact the case: codes that did not estimate masses according to the standard definition $M(<R) = 4\pi/3\,R^3\,\Delta\rho$ nevertheless recovered the correct v_{max} values. Given the ability of comparing v_{max} to observational data (cf. Section 1.3), we conclude that v_{max} is a more meaningful quantity which can serve as a proxy for mass. Note again the flattening of some curves at the low-v_{max} end due to either the resolution of the simulation analysed or an imposed minimum number of particles cut and that not all FOF-based finders returned a v_{max} value.

We have seen in Section 4.1 that there exists some scatter between halo finders in the recovery of the halo position. It therefore appears mandatory to check for differences in halo positions recovered from the cosmological simulation, too. To this extent, we calculated the
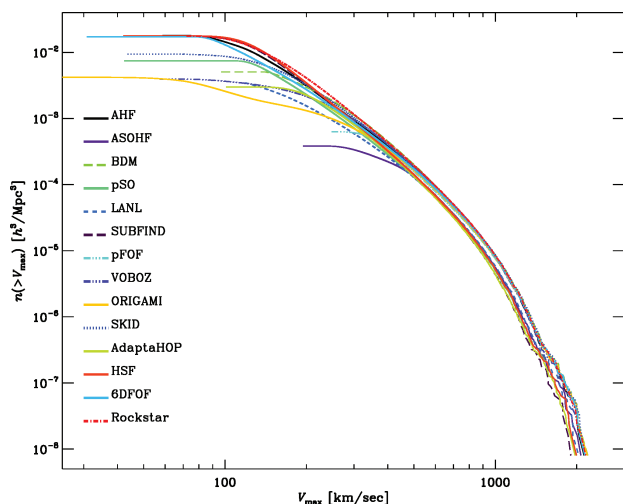
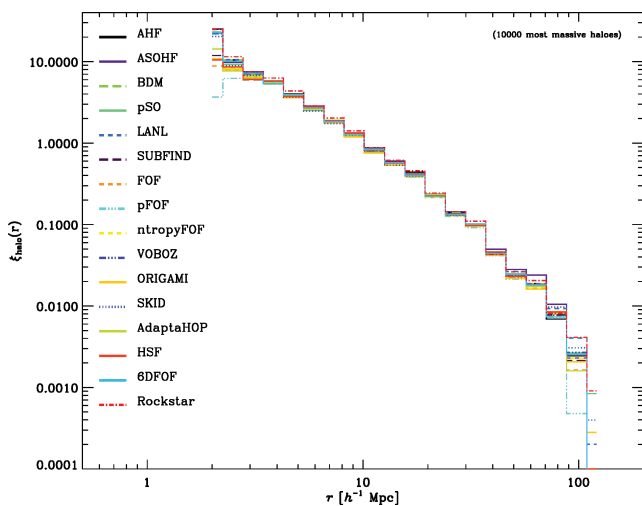**Figure 18.** The cumulative v_{max} function.

Figure 19. The two-point correlation function for the 10 000 most massive objects.

Figure 20. The distribution of bulk velocities for objects more massive than $5 \times 10^{11} \, h^{-1} \, \mathrm{M}_\odot$.

two-point correlation function and present the results in Fig. 19. In order to analyse a comparable data set (remember that some codes analysed the 1024^3, some the 512^3 and some the 256^3 particle simulation), we restricted the haloes to the 10 000 most massive objects and found excellent agreement.[12] The smallest scale considered in this comparison is $2 \, h^{-1}$ Mpc in order not to probe the interiors of galaxy clusters. The minute drop of the correlation function for PFOF at the smallest scale probed may be explained by the usage of the marginally larger linking length of $b = 0.2$ applied during their analysis and the fact that PFOF uses the centre of mass instead of the density peak as the centre of the halo.

Finally, we cross-compare the bulk velocities of haloes in Fig. 20 where we find excellent agreement. We further give in the legend the medians of the distribution for each halo finder: the mean (of

the medians) is 489 km s^{-1} with a 1σ of 9 km s^{-1} (i.e. 2 per cent deviation).

5 SUMMARY AND CONCLUSIONS

We have performed an exhaustive comparison of 18 halo finders for cosmological simulations. These codes were subjected to various suites of test scenarios all aimed at addressing issues related to the subject of identifying gravitationally bound objects in such simulations.

The tests consisted of idealized mock haloes set up according to a specific matter density profile (i.e. NFW and Plummer) where we studied isolated haloes as well as (sub-)subhaloes. We further utilized a cosmological simulation of the large-scale structure of the universe primarily containing field haloes. The requirement for the mock haloes was to simply return the centres of the identified objects alongside a list of particles (possibly) belonging to that halo. We then applied a universal tool to calculate all other quantities [e.g. bulk velocity, rotation curve, (virial) mass, etc.]. For the cosmological data, the code representatives were simply asked to return their 'best' values for a suite of canonical values.

Mock haloes. We found that the deviation of the recovered position to the actual centre of the object is largest for FOF-based methods which is naturally explained by the fact that they define centres as the centre of mass, whereas most other codes identify a peak in the density field. Further, DM haloes that have an intrinsic core (e.g. a Plummer sphere) yield larger differences between the input centre and the recovered centre for most codes. Such density profiles are not expected within the Universe we inhabit. However, the bulk velocities, (virial) masses and v_{max} values satisfactorily agreed with the analytical input, irrespective of the underlying density profile – at least for hosts and subhaloes; subsubhaloes still showed at times departures as large as 50 per cent in mass and 20 per cent for v_{max}. Note that all results are based upon the same post-processing software and only the list of particles (and the centre) was determined by each halo finder individually. Hence, variations in the centre will automatically lead to differences as both the mass and rotation curve are spherically averaged quantities.

We further investigated the dependence of subhalo properties upon the position within the host, in particular its distance from the

---

[12] Note that it makes little difference to use the 10 000 objects with the largest v_{max} value as there is a strong correlation between M and v_{max} for each code. At the end, we are interested in limiting the analyses to the N most massive objects and hence a 'miscalculation' of the mass is irrelevant as long as differences in mass are systematic as in our case.

centre. There we found that – while all codes participating in this exercise recovered excellent v_{max} values for a NFW subhalo sampled with 10 000 particles inside a NFW host two orders of magnitude more massive[13] – phase-space finders excelled by also locating the subhalo when it overlapped with the centre of the host. However, in this case they struggle to properly calculate its properties.

Putting a subhalo at varying positions inside a host is closely related to a subhalo actually falling into a host. However, the latter also introduces distortions in the shape of the subhalo due to tidal forces while it is plunging through the background potential of the host. We performed a simulation of the scenario where a subhalo initially containing 10 000 particles shoots right through the centre of a host two orders of magnitude more massive. While we found that the number of particles significantly drops when the subhalo approaches the host's centre, it rises again to a plateau level after the central passage – and this is apparent in all codes. The peak of the rotation curve, which should be less susceptible to (tidally induced) variations in the outer subhalo regions, shows less variation. However, v_{max} actually rises shortly after the subhalo leaves the very central region indicative of two (related) effects: contamination with host particles and problems with the unbinding procedure. Nevertheless, these problems are (still) common to all halo finders used in this particular study and they all mutually agree upon the initial and final values.

Another question addressed during our tests with the mock haloes was the number of particles required in a subhalo in order to still be able to separate it from the host background. To this extent, we successively lowered the number of particles used to sample a subhalo that had been placed at half the M_{100} radius of the host. We found that the majority of finders participating in this exercise are capable of identifying the subhalo down to 30–40 particles. Yet again, (most of) the phase-space finders even locate the object with as few as 10–20 particles. Some of the configuration space finders also tracked down the subhalo to such low numbers of particles; however, they did not obtain the correct particle lists leading to subhalo properties that differ from the analytical input values.

We would like to close this part of the summary with the notion that while there is a straightforward relation between the (virial) mass and the peak of the rotation curve for isolated field haloes (once the density profile is known), the mass of a subhalo is more ambiguously defined. As we have seen, it is (in most situations) more meaningful to utilize the peak of the rotation curve as a proxy for mass (cf. Fig. 8 versus Fig. 9 as well as Fig. 10 versus Fig. 11). However, as could also be witnessed in Fig. 11, quite a number of halo-finding techniques gave rise to an artificial increase in v_{max} right after the passage through the centre of its host, obscuring its applicability as a mass representative.

Cosmological simulation. As a matter of fact there is little to say regarding the comparison of the cosmological data sets; as can be seen in Figs 17–20, the agreement is well within the (omitted) error bars for the basic properties investigated here (i.e. mass, velocity, position and v_{max}), and unless we can be certain which halo-finding technique is the ultimate (if such exists at all), the observed scatter indicates the accuracy to which we can determine these properties in cosmological simulations. We would though like to caution that the haloes found within the cosmological simulation are primarily well-defined and isolated objects and hence it is no surprise that we find such an agreement. Subhaloes, however, are not well defined

and therefore lead to larger differences between halo finders as seen during the comparison of the mock haloes. For those codes that diverge from the general agreement, the differences are readily explained and have been discussed in Section 4.2.

Concluding remarks. The agreement amongst the different codes is rather remarkable and reassuring. While they are based upon different techniques and – even for those based upon the same technique – different technical parameters, they appear to recover comparable properties for DM haloes as found in state-of-the-art simulations of cosmic structure formation. We nevertheless need to acknowledge that some codes require improvement. For instance, phase-space finders find halo centres even if the centre overlaps with another (distinct) object and recover subhaloes to a smaller particle number; however, they still have problems with the (separated) issue of assigning the correct particles in these cases and hence deriving halo properties afterwards.

We close with the remark that we deliberately did not dwell on the actual technical parameters of each and every halo finder as this is beyond the scope of this paper and we refer the reader to the respective code papers for this. However, it is important to note that with an appropriate choice of these parameters the results can be brought into agreement. This is an important message from this particular study. We are not claiming that all halo finders need to return identical results, but they can (possibly) be tuned that way. In that regard, we also like to remind the reader again that this particular comparison is aimed at comparing codes as opposed to algorithms: we even tried to gauge the differences found when applying codes based upon the same algorithm to identical data sets.

---

[13] Note that only halo finders capable of identifying substructures can participate in a comparison of (sub-)subhalo properties.

REFERENCES

Agertz O. et al., 2007, MNRAS, 380, 963
Ascasibar Y., Binney J., 2005, MNRAS, 356, 872
Ascasibar Y., Gottlöber S., 2008, MNRAS, 386, 2022
Aubert D., Pichon C., Colombi S., 2004, MNRAS, 352, 376
Bagla J. S., Khandai N., 2009, MNRAS, 396, 2211
Barnes J., Hut P., 1986, Nat, 324, 446
Bertschinger E., Gelb J. M., 1991, Comput. Phys., 5, 164
Binney J., Tremaine S., 1987, Galactic Dynamics. Princeton Univ. Press, Princeton, NJ
Bode P., Ostriker J. P., Xu G., 2000, ApJS, 128, 561
Bullock J. S., Kolatt T. S., Sigad Y., Somerville R. S., Kravtsov A. V., Klypin A. A., Primack J. R., Dekel A., 2001, MNRAS, 321, 559
Cohn J. D., White M., 2008, MNRAS, 385, 2025
Couchman H. M. P., Thomas P. A., Pearce F. R., 1995, ApJ, 452, 797
Courtin J., Rasera Y., Alimi J., Corasaniti P., Boucher V., Füzfa A., 2011, MNRAS, 410, 1911
Davis M., Efstathiou G., Frenk C. S., White S. D. M., 1985, ApJ, 292, 371
Dekel A., Devor J., Hetzroni G., 2003, MNRAS, 341, 326
Diemand J., Kuhlen M., Madau P., 2006, ApJ, 649, 1
Doumler T., Knebe A., 2010, MNRAS, 403, 453
Dubinski J., Kim J., Park C., Humble R., 2004, New Astron., 9, 111
Eisenstein D. J., Hut P., 1998, ApJ, 498, 137
Frenk C. S. et al., 1999, ApJ, 525, 554
Fryxell B. et al., 2000, ApJS, 131, 273
Gardner J. P., Connolly A., McBride C., 2007a, Broadening Participation in the TeraGrid Enabling Knowledge Discovery in a Virtual Universe. ACM Press, Madison, WI
Gardner J. P., Connolly A., McBride C., 2007b, Challenges of Large Applications in Distributed Environments (CLADE 2007) Enabling Rapid Development of Parallel Tree Search Applications. ACM Press, Monterey, CA
Gelb J. M., 1992, PhD thesis, Massachusetts Institute of Technology
Gelb J. M., Bertschinger E., 1994, ApJ, 436, 467
Gill S. P. D., Knebe A., Gibson B. K., 2004, MNRAS, 351, 399
Gnedin N. Y., 1995, ApJS, 97, 231
Gottlöber S., Yepes G., 2007, ApJ, 664, 117
Gottlöber S., Klypin A. A., Kravtsov A. V., 1999, in Giuricin G., Mezzetti M., Salucci P., eds, ASP Conf. Ser. Vol. 176, Observational Cosmology: The Development of Galaxy Systems. Astron. Soc. Pac., San Francisco, p. 418
Governato F., Moore B., Cen R., Stadel J., Lake G., Quinn T., 1997, Nat, 2, 91
Habib S. et al., 2009, J. Phys. Conf. Ser., 180, 012019
Hayashi E., Navarro J. F., Taylor J. E., Stadel J., Quinn T., 2003, ApJ, 584, 541
Heitmann K. et al., 2008, Comput. Sci. Discovery, 1, 015003
Hernquist L., 1990, ApJ, 356, 359
Hernquist L., 1993, ApJS, 86, 389
Jenkins A., Frenk C. S., White S. D. M., Colberg J. M., Cole S., Evrard A. E., Couchman H. M. P., Yoshida N., 2001, MNRAS, 321, 372

Kazantzidis S., Magorrian J., Moore B., 2004, ApJ, 601, 37
Kim J., Park C., 2006, ApJ, 639, 600
Klimentowski J., Łokas E. L., Kazantzidis S., Mayer L., Mamon G. A., 2009, MNRAS, 397, 2015
Klypin A., Holtzman J., 1997, preprint (arXiv e-prints)
Klypin A., Gottlöber S., Kravtsov A. V., Khokhlov A. M., 1999, ApJ, 516, 530
Knebe A., Kravtsov A. V., Gottlöber S., Klypin A. A., 2000, MNRAS, 317, 630
Knebe A., Green A., Binney J., 2001, MNRAS, 325, 845
Knollmann S. R., Knebe A., 2009, ApJS, 182, 608
Kravtsov A. V., Klypin A. A., Khokhlov A. M., 1997, ApJS, 111, 73
Kruskal Joseph B. J., 1956, Proc. Am. Math. Soc., 7, 48
Lacey C., Cole S., 1994, MNRAS, 271, 676
Łokas E. L., Mamon G. A., 2001, MNRAS, 321, 155
Lukić Z., Heitmann K., Habib S., Bashinsky S., Ricker P. M., 2007, ApJ, 671, 1160
Lukić Z., Reed D., Habib S., Heitmann K., 2009, ApJ, 692, 217
Lux H., Read J. I., Lake G., 2010, MNRAS, 406, 2312
Maciejewski M., Colombi S., Springel V., Alard C., Bouchet F. R., 2009, MNRAS, 396, 1329
Merz H., Pen U., Trac H., 2005, New Astron., 10, 393
More S., Kravtsov A., Dalal N., Gottlöber S., 2011, preprint (arXiv e-prints)
Muldrew S. I., Pearce F. R., Power C., 2011, MNRAS, 410, 2617
Navarro J. F., Frenk C. S., White S. D. M., 1995, MNRAS, 275, 720
Navarro J. F., Frenk C. S., White S. D. M., 1996, ApJ, 462, 563
Navarro J. F., Frenk C. S., White S. D. M., 1997, ApJ, 490, 493
Navarro J. F. et al., 2010, MNRAS, 402, 21
Neyrinck M. C., Gnedin N. Y., Hamilton A. J. S., 2005, MNRAS, 356, 1222
O'Shea B. W., Bryan G., Bordner J., Norman M. L., Abel T., Harkness R., Kritsuk A., 2004, preprint (arXiv e-prints)
O'Shea B. W., Nagamine K., Springel V., Hernquist L., Norman M. L., 2005, ApJS, 160, 1
Pen U., 1995, ApJS, 100, 269
Pfitzner D. W., Salmon J. K., 1996, Parallel Halo Finding in N-body Cosmology Simulations. Astron. Rechen-Institut. Heidelberg, Germany
Planelles S., Quilis V., 2010, A&A, 519, A94
Plummer H. C., 1911, MNRAS, 71, 460
Press W. H., Schechter P., 1974, ApJ, 187, 425
Quilis V., 2004, MNRAS, 352, 1426
Rasera Y., Alimi J., Courtin J., Roy F., Corasaniti P., Füzfa A., Boucher V., 2010, in Alimi J.-M., Fuözfa A., eds, AIP Conf. Ser. Vol. 1241, Invisible Universe. Am. Inst. Phys., New York, p. 1134
Read J. I., Wilkinson M. I., Evans N. W., Gilmore G., Kleyna J. T., 2006, MNRAS, 367, 387
Read J. I., Lake G., Agertz O., Debattista V. P., 2008, MNRAS, 389, 1041
Robertson B. E., Kravtsov A. V., Tinker J., Zentner A. R., 2009, ApJ, 696, 636
Schaap W. E., van de Weygaert R., 2000, A&A, 363, L29
Sharma S., Steinmetz M., 2006, MNRAS, 373, 1293
Shaw L. D., Weller J., Ostriker J. P., Bode P., 2007, ApJ, 659, 1082
Sheth R. K., Tormen G., 1999, MNRAS, 308, 119
Shiloach Y., Vishkin U., 1982, J. Algorithms, 3, 57
Skory S., Turk M. J., Norman M. L., Coil A. L., 2010, ApJS, 191, 43
Springel V., 2005, MNRAS, 364, 1105
Springel V., 2010, MNRAS, 401, 791
Springel V., White S. D. M., Tormen G., Kauffmann G., 2001a, MNRAS, 328, 726
Springel V., Yoshida N., White S. D. M., 2001b, New Astron., 6, 79
Stadel J. G., 2001, PhD thesis, Univ. Washington
Stadel J., Potter D., Moore B., Diemand J., Madau P., Zemp M., Kuhlen M., Quilis V., 2009, MNRAS, 398, L21
Sutter P. M., Ricker P. M., 2010, ApJ, 723, 1308
Tasker E. J., Brunino R., Mitchell N. L., Michielsen D., Hopton S., Pearce F. R., Bryan G. L., Theuns T., 2008, MNRAS, 390, 1267

Teyssier R., 2002, A&A, 385, 337

Tinker J., Kravtsov A. V., Klypin A., Abazajian K., Warren M., Yepes G., Gottlöber S., Holz D. E., 2008, ApJ, 688, 709

Tweed D., Devriendt J., Blaizot J., Colombi S., Slyz A., 2009, A&A, 506, 647

van Kampen E., 1995, MNRAS, 273, 295

Warren M. S., Abazajian K., Holz D. E., Teodoro L., 2006, ApJ, 646, 881

Weller J., Ostriker J. P., Bode P., Shaw L., 2005, MNRAS, 364, 823

White M., 2001, A&A, 367, 27

White M., 2002, ApJS, 143, 241

Zemp M., Moore B., Stadel J., Carollo C. M., Madau P., 2008, MNRAS, 386, 1543

This paper has been typeset from a TEX/LATEX file prepared by the author.